

Lattice Boltzmann study of mass transfer for two-dimensional Bretherton/Taylor bubble train flow

A. Kuzmin^{a,*}, M. Januszewski^{b,d}, D. Eskin^c, F. Mostowfi^c, J.J. Derksen^a

^a*Chemical and Materials Engineering, University of Alberta
7th Floor, ECERF, 9107 116 St, Edmonton, Alberta, T6G 2V4 Canada*

^b*Institute of Physics, University of Silesia, 40-007 Katowice, Poland*

^c*Schlumberger DBR Technology Center
9450 17 Ave NW, Edmonton, Alberta, T6N 1M9 Canada*

^d*Google Switzerland GmbH, Brandschenkestrasse 110, 8002 Zurich, Switzerland*

Abstract

This work presents a procedure for the determination of the volumetric mass transfer coefficient in the context of lattice Boltzmann simulations for the Bretherton/Taylor bubble train flow for capillary numbers $0.1 < Ca < 1.0$. We address the case where the hydrodynamic pattern changes from having a vortex in a slug ($Ca < 0.7$) to not having it ($Ca > 0.7$) [?]. In the latter case the bubble shape is asymmetric and cannot be approximated through flat surfaces and circular circumferences as is often done in the literature [? ?]. When the vortex is present in the slug, the scalar concentration is well mixed and it is common to use periodic boundary conditions and the inlet/outlet-averaged concentration as the characteristic concentration. The latter is not valid for flows where the tracer is not well mixed, i.e. $Ca > 0.7$. We therefore examine various boundary conditions (periodic, open, open with more than 1 unit cell) and definitions of the characteristic concentration to estimate mass transfer coefficients for the range of capillary numbers $0.1 < Ca < 1.0$. We show that the time-dependent volume averaged concentration taken as the characteristic concentration produces the most robust results and that all strategies presented in the literature are extreme limits of one unified equation. Finally, we show good agreement of simulation results for different

*Corresponding author

Email addresses: kuzmin@ualberta.ca (A. Kuzmin), michal.j@gmail.com (M. Januszewski), deskin@slb.com (D. Eskin), fmostowfi@slb.com (F. Mostowfi), jos@ualberta.ca (J.J. Derksen)

Peclet numbers with analytical predictions of [?].

Keywords: Mass Transfer, Taylor/Bretherton bubble train flow, Multiphase flow, Lattice Boltzmann method, Binary liquid model, Flow in microchannels with parallel plates

1. Introduction

Monolith reactors have recently been getting more attention as a promising alternative to slurry reactors and trickle bed reactors [? ?]. These reactors usually operate in the Bretherton-Taylor regime [? ?] which is a flow of equally sized, long air bubbles through a liquid medium, see Fig. ???. This flow regime is characterized by the dominance of surface tension over inertia and viscous effects, and by comparatively small gas flow velocities [?]. Due to the dominance of surface tension, the flow exhibits advantageous properties which cannot be achieved in its macroscopic counterparts: liquid thin films [?] between bubbles and walls strongly enhance mass transfer from gas and walls to liquid; the plug flow regime occurring in monolith reactors allows to perform chemical reactions in slugs only [?]. Moreover, the low slip velocity between gas and liquid is utilized in experiments to measure liquid velocity [?]: bubbles travelling with approximately the same velocity as liquid can be captured with a camera. These properties explain why nowadays one can find a large number of applications of the Bretherton-Taylor bubble train flow: continuous flow analyzers to measure liquid velocity, chemical reactors for hydrogenation of nitroaromatics, 2-ethyl-hexenal, Fischer-Tropsch synthesis, etc. The extensive reviews of [? ? ?] cover a significant number of applications.

This work is focused on gas to liquid mass transfer for the two-dimensional Bretherton/Taylor flow. A good understanding of mass transfer and how it depends on parameters such as the capillary number, the Reynolds number, and slug and bubble lengths allows to properly manufacture a microchannel with properties necessary to ensure that chemical reactions are performed in the best possible manner. The mass transfer coefficient is defined as the flux from the gas-liquid interface divided by the difference of the imposed concentration and the characteristic concentration in the domain. The concentration distribution in the domain is prescribed by underlying hydrodynamics fields. For example, experimental studies [? ?] show a complex dependency of the mass transfer coefficient on flow parameters: bubble and slug lengths,

and bubble velocity, which in turn relate to the capillary number Ca and the Reynolds number Re . [?] established an experimental correlation for the volumetric mass transfer coefficient for a bubble train as a function of the diffusion coefficient, slug and bubble lengths, and bubble velocity:

$$k_L a = \frac{2}{d_h} \left(\frac{DU_{\text{bubble}}}{L_{\text{bubble}} + L_{\text{slug}}} \right)^{0.5} \left(\frac{L_{\text{bubble}}}{L_{\text{bubble}} + L_{\text{slug}}} \right)^{0.3}, \quad (1)$$

where $k_L a$ is the volumetric mass transfer coefficient, d_h is the hydraulic diameter, L_{bubble} is the bubble length, L_{slug} is the slug distance (between bubbles), U_{bubble} is the bubble velocity, and D is the diffusion coefficient.

The understanding of mass transfer for the bubble train flow is not possible without knowledge of hydrodynamic patterns. There are several works studying the hydrodynamic properties of the bubble train flow, both experimental [?] and numerical [?]. For the flow of long bubbles between parallel plates chosen here as the study case, it is indicated that there exists a vortex in the liquid slug for $Ca < 0.7$, see Fig. ??, and that the bubble shape is symmetric for low capillary numbers ($Ca < 0.1$ [?]) with the capillary number defined as:

$$Ca = \frac{\mu_{\text{liq}} U_{\text{bubble}}}{\gamma}, \quad (2)$$

where μ_{liq} is the liquid viscosity, U_{bubble} is the bubble velocity, and γ is the interfacial tension. The fact that the bubble shape for $Ca < 0.1$ can be represented as two hemicircles and two planar interfaces with the vortex existing in the liquid slug has been utilized for analytical estimations of mass transfer properties.

Since the mass transfer coefficient is defined in terms of a mass flux through a certain area, Eq. ??, analytical estimates [?] are based on a decomposition of the bubble surface in parts. The mass transfer coefficient is calculated through two separate contributions from two planar films and two hemicircles. For both contributions the Higbie penetration theory [?] is utilized, which states that the mass transfer coefficient for a simple flow geometry depends on the average time a liquid packet interacts with a geometrical feature. It can be calculated as $\sqrt{\frac{\pi D}{t_{\text{char}}}}$, where t_{char} is the interaction time. As an example of the application of the Higbie penetration theory, the mass transfer coefficient for the flow of bubbles between parallel plates

is calculated as (similar to the work of [?]):

$$k_L = 2\sqrt{\frac{\pi D}{t_{\text{film}}}} + 2\sqrt{\frac{\pi D}{t_{\text{circle}}}}, \quad (3)$$

where $t_{\text{film}} = \frac{L_{\text{film}}}{U_{\text{bubble}}}$ stands for the interaction time of liquid traveling next to the planar part of the bubble, and $t_{\text{circle}} = \frac{\pi R_{\text{circle}}}{U_{\text{bubble}}}$ is the time during which the liquid in the slug travels the distance of half the bubble cap circumference.

Despite their simplicity, such analytical expressions work well for flows with low capillary numbers $Ca < 0.1$ [?] where the bubble shape is symmetrical and can be approximated with good precision. Moreover, because of the hydrodynamic pattern in the slug (i.e. presence of a vortex in slug), one can estimate the time for a fluid batch to travel the whole circumference. However, with the increase of the capillary number the situation changes significantly – the symmetrical bubble shape is lost and the bubble resembles a bullet [?]. For flows with $Ca > 0.7$ there is also no vortex in the liquid slug. In this case the Higbie theory fails to estimate the contribution from bubble caps, which explains the need to turn to numerical simulations where all hydrodynamic fields as well as complex bubble shapes are taken into account.

Typical numerical studies of mass transfer [? ?] do not consider the simulation of bubble shapes for $Ca > 0.1$. The usual simulation of mass transfer is performed as follows:

I The bubble shape is calculated either through analytical correlations [?] or experimental correlations [?] without directly resolving bubble shapes through multiphase simulations. The expressions for bubble shapes are available only for flows with capillary number $Ca < 0.1$.

II Hydrodynamic fields are then obtained by performing simulations of one-component flow around the bubble by imposing the bubble velocity on the channel walls. Thus, the simulations are performed in the reference frame moving with the bubble. A stress-free condition is imposed at the bubble surface.

III The mass transfer simulations are performed in the reference frame moving with the bubble. The saturation concentration is imposed at the bubble surface. Only one unit cell containing a single bubble is used for simulations. Periodic concentration boundary conditions are utilized to

determine the volumetric mass transfer coefficient, which is calculated through the following equation [?]:

$$k_L a = \frac{\overline{\text{Flux}}}{C_{\text{bubble}} - \langle C_{\text{in/outlet}} \rangle} \frac{\text{bubble surface area}}{\text{unit cell volume}}, \quad (4)$$

where $\langle C_{\text{in/outlet}}(t) \rangle = \int C U_{\text{in/outlet}} dA / \int U_{\text{in/outlet}} dA$ is the space-averaged inlet/outlet (periodic boundary conditions) concentration as a function of time. Therefore, in terms of the mass transfer definition, $\langle C_{\text{in/outlet}}(t) \rangle$ plays the role of the characteristic concentration. The time-averaged concentration flux ($\overline{\text{Flux}}$) is calculated as the difference between the overall average concentration in the whole domain ($\langle C_{\text{overall}} \rangle = \int_V C dV / V$) at time t_1 and at time t_2 divided by the time difference $t_2 - t_1$. The agreement between numerical simulations [?] and experimental correlations of [?] was good.

The presented numerical approaches [? ?] can be criticized on a number of points. They mainly relate to the bubble shape approximation, which is taken to be symmetrical, i.e. consisting of two hemispheres and film for the case of flow in circular capillaries. This is valid for small capillary numbers only ($Ca < 0.1$). As previously discussed, for such capillary numbers the tracer is well mixed in the slug and the choice of the characteristic concentration needed for the mass transfer coefficient, Eq. ??, is obvious. With minimal differences in the results, it can either be the averaged concentration in the liquid slug or the inlet/outlet space-averaged concentration. The latter is used in the formulation of [?] presented above.

While it is clear that periodic boundary conditions can be employed for the calculation of hydrodynamic fields, the same does not apply to the mass transfer coefficient simulations. Experimental correlations [?] show that the concentration in a bubble train along the streamwise direction changes exponentially with distance. Mass transfer simulations however, are made only for one unit cell using periodic boundary conditions with the same concentration at the inlet and at the outlet. The question is how single unit cell simulation corresponds to experimental measurements arises where concentration difference is measured at the distances of at least a few unit cells [?]. In other words, one needs to understand how the discrete one unit cell simulation corresponds to the continuous picture in experiments where one does not distinguish discrete bubbles but takes measurements of concentration at different locations.

Addressing situations for a rich number of hydrodynamic patterns, shapes, and effects of bubble lengths, etc for bubble train flows, we feel that there is a need to examine carefully the strategies and assumptions behind the numerical calculations of the mass transfer coefficient. We aim at establishing clear procedures as to how properly obtain the mass transfer coefficient via a study of different boundary conditions and different definitions of the characteristic concentration. The case we want to examine is a two-dimensional bubble train flow between parallel plates. We address the following issues:

I Applicability of periodic boundary conditions to determine the mass transfer coefficient when the vortex in the slug disappears, i.e. when $Ca > 0.7$.

II Validity of the inlet/outlet-averaged or domain-averaged concentrations as characteristic concentrations in the definition of the mass transfer coefficient.

III Translation of the continuous experimental picture to numerical simulations of a few unit cells, the issue of correspondence between space averages (simulations [?]) and time averages (experiment).

In addition, at the end of the manuscript we present results of the dependence of the volumetric mass transfer coefficient on the Peclet number that we compare with analytical [?] and experimental correlations [?]. The thorough determination of the mass transfer coefficient and associated Sherwood number as a function of other non-dimensional parameters such as gas holdup, bubble/slug lengths, and the capillary number is left for future studies.

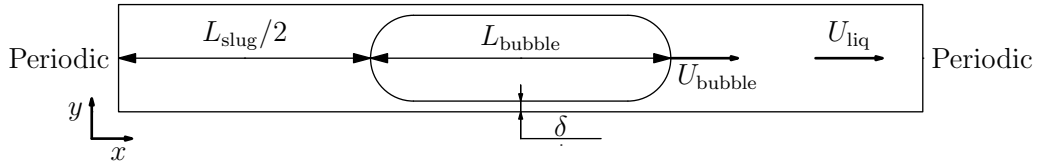


Figure 1: Simplified sketch of the bubble motion. Using periodic conditions for the velocity field is natural, but needs evaluation for mass transfer.

To establish numerical procedures we performed multiphase simulations to extract bubble shapes [? ?] for the range of capillary numbers $Ca = 0.1 \div 1.0$. For this range of capillary numbers we were able to capture the

115 bubble shape change and the change of hydrodynamic patterns. The mass
 116 transfer simulations presented here were performed with various boundary
 117 conditions (open, periodic) and with a few unit cells (1 to 10 unit cells). As
 118 our numerical approach we take the lattice Boltzmann method, a relatively
 119 new CFD competitor developed during last 20 years [? ? ? ?]. This method
 120 was successfully applied to simulate not only single phase hydrodynamic
 121 problems [?], but also multiphase flows [? ? ?], heat transfer [? ?], and
 122 ferrofluids [? ?].

123 Mass transfer problems in the lattice Boltzmann framework were mainly
 124 addressed in a series of works of Ginzburg and co-authors [? ? ?]. In con-
 125 trast to these works whose focus was on simulating the advection-diffusion
 126 equation via the lattice Boltzmann framework, we concentrate on the appli-
 127 cation side. One should also mention the work of ?] about heat and mass
 128 transfers in porous media and the work of ?] simulating lateral mixing in
 129 cross-channel flow. The last two works are focused on problems of homo-
 130 geneous nature and do not provide guidance as to how to obtain the mass
 131 transfer coefficient for heterogeneous cases.

132 The paper is organized as follows. We start with definitions of the volu-
 133 metric mass transfer coefficient and apply them to the bubble train flow to
 134 derive expressions to connect the space- and time-averages. Then, the lattice
 135 Boltzmann model used to simulate mass transfer is presented, followed by
 136 benchmarks. Finally, numerical simulations of various boundary conditions
 137 and simulations spanning a few unit cells for different hydrodynamic pat-
 138 terns are presented to establish the procedure to determine the volumetric
 139 mass transfer coefficient. The comparison with analytical correlations is also
 140 presented.

141 2. Mass transfer definitions

By definition, the mass transfer coefficient from a surface with an imposed
 constant concentration C_{bubble} is:

$$k_L = \frac{\dot{m}}{P\Delta C}, \quad \Delta C = C_{\text{bubble}} - C_{\text{medium}}, \quad (5)$$

142 where \dot{m} is the mass flux $\left[\frac{kg}{s}\right]$, P is the area of the surface $\left[m^2\right]$, and ΔC is
 143 the concentration difference between the surface and the surrounding medium
 144 $\left[\frac{kg}{m^3}\right]$. Therefore, k_L has a dimension of $\left[\frac{m}{s}\right]$. Usually, the surrounding

medium concentration is taken at an infinite distance from the bubble. However, in the case of complicated geometries and non-homogeneous concentrations, the medium concentration can be the average concentration in the domain or the flux-averaged concentration at the inlet or outlet, etc. Thus, one needs to establish a clear definition of ΔC to determine the volumetric mass transfer coefficient in the case of complex geometries and non-trivial hydrodynamic velocity patterns.

We first examine the definitions of mass transfer in the case of point sources.

2.1. Point mass sources

In what follows we will present three approaches to calculate point mass transfer coefficients (by point source we assume the source to have an infinitesimally small surface area P):

1. Let us look at the infinitesimally small domain of volume $A\Delta x$, not moving and containing a point source. The concentration difference is $\Delta C = C^* - C(t)$, where C^* is the imposed point source concentration, and $C(t)$ is the time-dependent concentration, which does not depend on the location due to the assumption of homogeneity. One can therefore write a time-dependent ordinary differential equation for the concentration in the domain:

$$\dot{m} = A\Delta x \frac{dC}{dt} = k_L P (C^* - C(t)), \quad (6)$$

with the initial condition $C(0) = 0$. The solution can be found as:

$$C(t) = C^*(1 - \exp(-k_L a t)), \quad (7)$$

where $k_L a$ is the volumetric mass transfer coefficient defined as:

$$k_L a = k_L \frac{P}{A\Delta x} = k_L \frac{P}{V}, \quad (8)$$

where P is the source surface, V is the unit cell volume.

2. Let us predict mass transfer in a liquid moving with the velocity U , see Fig. ??.

If one can assume that the point mass sources are distributed in the whole medium, the mass accumulated in the volume $V = A\Delta x$ can be calculated as the difference of mass fluxes entering and leaving the

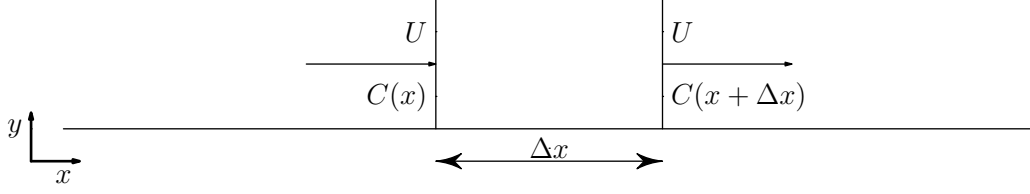


Figure 2: The mass transfer in a moving liquid.

domain $U(C(x + \Delta x) - C(x))$. The accumulated mass should be proportional to the mass transfer coefficient:

$$U(C(x + \Delta x) - C(x)) = k_L P(C^* - C(x)), \quad (9)$$

giving the same solution but only in the spatial domain:

$$C(x) = C^* \left(1 - \exp\left(-k_L a \frac{x}{U}\right) \right). \quad (10)$$

161 Note that the concentration $C(x)$ does not depend on time.

- 162 3. If one transfers to the frame moving with the liquid velocity U , the
 163 situation will be the same as in the first case. One can connect time
 164 and space with the velocity U ($t = \frac{x}{U}$) to obtain the same equation as
 165 in the case 2.

166 2.2. Bubble train

167 In the application to the bubble train flow it is useful to think of one
 168 bubble as a point source to be able to use the calculations presented above.
 169 For example, the expression (??) was used in experiments by ?]. However,
 170 one should be accurate with the definition of velocities because two different
 171 phases co-exist in the bubble train flow. Usually, one can take the velocity
 172 U to be a bulk velocity or $U = U_{\text{gas}} + U_{\text{liq}}$, where U_{gas} and U_{liq} are liquid and
 173 gas superficial velocities, respectively.

174 With experimental measurements of concentration at different locations,
 175 the calculation of the mass transfer coefficient using the logarithmic func-
 176 tion is straightforward. However, if one wants to analytically or numerically
 177 calculate the mass transfer coefficients, the situation is much more compli-
 178 cated because of the presence of two phases and complex bubble geometry.
 179 As was mentioned before, depending on the capillary number the velocity
 180 pattern and thus scalar mixing is different. Analytical approaches [? ?]

181 assume that the contributions from film and bubble caps can be calculated
182 separately. Therefore no tracer from the film influences bubble caps diffu-
183 sion. However, this assumption overpredicts mass transfer for a number of
184 experiments [?]. This happens since some tracer concentration from the
185 film is mixed with the slug and increases the overall concentration in the
186 slug, thereby decreasing the mass transfer from the bubble caps. Therefore,
187 the analytical estimates for the mass transfer coefficient calculation do not
188 account for mutual mass transfer from neighbouring bubbles.

189 Overall, mixing patterns of the film and liquid slugs are of great impor-
190 tance for the estimation of mass transfer [?]. However, the assumptions
191 usually taken for mass transfer calculations are small capillary numbers and
192 certain mixing patterns such as to help to estimate the mass transfer using
193 the penetration theory of ?].

194 In comparison with analytical calculations and simplifications, the nu-
195 merical approach can take into account the complex mixing patterns and
196 geometries. However, there are challenges as how to mimic the continuous
197 picture where the medium is moving with bulk velocity $U = U_{\text{gas}} + U_{\text{liq}}$ as
198 it is done in experiments. Thus, the questions indicated in Section 1 arise.
199 The next section gives more details about numerical simulations.

200 2.3. Numerical simulations

201 Ideally one wants to mimic the continuous picture as it is seen in ex-
202 periments. Thus, mass transfer simulations for a number of unit cells each
203 containing a bubble are needed. As was indicated above, there are two ap-
204 proaches towards it – either to simulate the bubble train and then to measure
205 concentration along the pipe, Eq. ??, or to transfer to the reference frame
206 moving with the bulk velocity U and conduct the same measurements. How-
207 ever, both methods require tracking of moving bubbles which is complicated
208 from the numerical point of view. Therefore, one needs to come up with a
209 simple and smaller domain for calculations of the mass transfer coefficient,
210 which closely mimics the continuous picture of a large number of separated
211 bubbles.

212 To avoid complications with moving grids, our approach is to simulate
213 mass transfer in a reference frame moving with the bubble. Therefore, one
214 needs to examine Eq. ?? more closely.

We perform simulations in the frame co-moving with the bubble in which
the bubble position stays constant. The bubble velocity U_{bubble} is different

from the bulk velocity $U = U_{\text{gas}} + U_{\text{liq}}$, and one thus needs to perform a x coordinate variable change:

$$\begin{aligned} x(t) &= U_{\text{bubble}} t \\ \overline{C(x)} &= C^* \left(1 - \exp\left(-k_L a \frac{x}{U_{\text{gas}} + U_{\text{liq}}}\right) \right) \\ \langle C(t) \rangle &= C^* \left(1 - \exp\left(-k_L a t \frac{U_{\text{bubble}}}{U_{\text{gas}} + U_{\text{liq}}}\right) \right), \end{aligned} \quad (11)$$

where $\langle C(t) \rangle$ is the space-averaged characteristic concentration, and $\overline{C(x)}$ is the time-averaged concentration at location x . One can make different choices for $\langle C(t) \rangle$ such as the concentration averaged over the whole domain or inlet/outlet space-averaged concentrations used in works [? ?]. The volumetric mass transfer coefficient can be obtained through the space-averaged concentration:

$$\begin{aligned} k_L a t \frac{U_{\text{bubble}}}{U_{\text{gas}} + U_{\text{liq}}} &= \ln \frac{C^*}{C^* - \langle C(t) \rangle} \\ k_L a \frac{L_{\text{unit}}}{U_{\text{bubble}} + U_{\text{gas}}} &= \frac{L_{\text{unit}}}{U_{\text{bubble}} t} \ln \frac{C^*}{C^* - \langle C(t) \rangle}, \end{aligned} \quad (12)$$

where the parameter $k_L a \frac{L_{\text{unit}}}{U_{\text{gas}} + U_{\text{liq}}}$ is non-dimensional. One can also measure the volumetric mass transfer coefficient from concentrations given at times t_1 and t_2 :

$$k_L a \frac{L_{\text{unit}}}{U_{\text{bubble}} + U_{\text{gas}}} = \frac{L_{\text{unit}}}{U_{\text{bubble}}(t_2 - t_1)} \ln \frac{C^* - \langle C(t_1) \rangle}{C^* - \langle C(t_2) \rangle}. \quad (13)$$

215 Expressions (?? - ??) are the cornerstones of the present work . Four possible
216 scenarios of numerical simulations have been examined:

- 217 1. One unit cell is simulated with periodic boundary conditions, see Fig.
218 ???. In this case no tracer leaves the domain similarly to the plug
219 flow. Though easier to implement, it gives rise to the criticism that
220 the inlet concentration is equal to the outlet one. As was discussed, in
221 experiments there is a concentration difference between the inlet and
222 the outlet, even for one unit cell.

In this case, the volumetric mass transfer coefficient is calculated by Eq. ???. The characteristic concentration $\langle C(t) \rangle$ required for the volumetric

mass transfer coefficient is taken as the average concentration in the domain:

$$C(t) = \frac{\int_{liquid} C dV}{\int dV}. \quad (14)$$

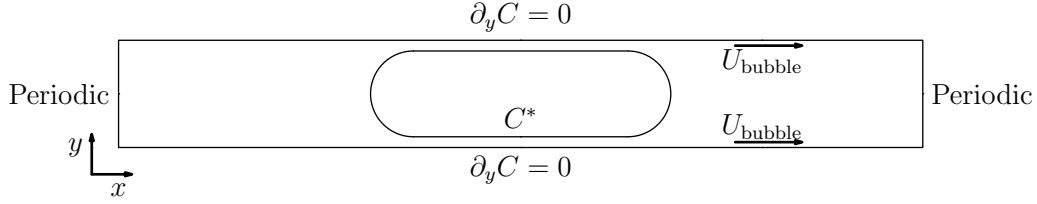


Figure 3: The two-dimensional benchmarks for the the mass transfer coefficient (bottom) for the bubble located near the entrance (top) and at the middle of the domain (bottom).

223

2. Periodic boundary conditions are applied as in the first case but the characteristic concentration is taken as the inlet/outlet flux-averaged concentration [?]:

$$\begin{aligned} \langle C_{inlet}(t) \rangle &= \frac{\int U(y)C(0, y, t)dy}{\int U(0, y)dy} \\ \langle C_{outlet}(t) \rangle &= \frac{\int U(y)C(L_{unit}, y, t)dy}{\int U(L_{unit}, y)dy} \\ C_{inlet}(\mathbf{x}, t) &= C_{outlet}(\mathbf{x}, t), \text{ due to periodicity.} \end{aligned} \quad (15)$$

224

225

226

227

The assumptions of this approach are that the concentration difference between the inlet/outlet- and the space-averaged over the whole unit cell is not significant. Thus, the tracer is assumed to be well mixed in the slug.

3. The approach of [?], where periodic boundary conditions are used and the mass transfer coefficient is calculated as the gain of the mass in the system divided by the concentration difference multiplied by the surface area:

$$k_L a = \frac{\dot{m}}{P \Delta C} \frac{P}{V} = \frac{\dot{m}}{V(C^* - \langle C(t) \rangle)}, \quad (16)$$

where the mass flux in the domain can be calculated as:

$$\dot{m} = \frac{m_2 - m_1}{t_2 - t_1} = \frac{\int_{liq} C(\mathbf{x}, t_2) d\mathbf{x} - \int_{liq} C(\mathbf{x}, t_1) d\mathbf{x}}{t_2 - t_1}. \quad (17)$$

228 In the approach of ? the inlet/outlet flux-averaged concentrations were
 229 taken as the characteristic concentration $\langle C(t) \rangle$.
 230 4. Simulation of several unit cells, see Fig. ?? . This situation corresponds
 231 to the head of the bubble train, after injection in the pipe and travel-
 232 ling along the channel. One can see that this situation best resembles
 233 the experimental picture, but also requires larger computational re-
 234 sources. By simulating a certain number of bubbles in the train head,
 235 the influence of the boundaries can be reduced. For example, left and
 236 right boundary conditions in this case are taken as open boundaries,
 237 i.e. $\partial C / \partial x = 0$. There is no ambiguity in the choice of the characteris-
 238 tic concentration. The average concentration of any unit cell far away
 from boundaries will be governed by Eq. ??.

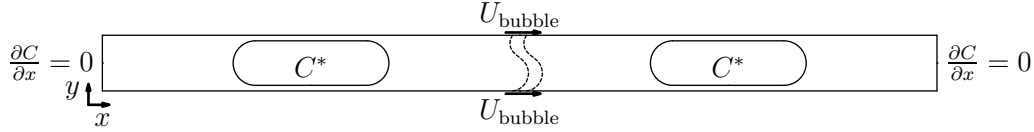


Figure 4: Benchmark for multiple unit cells.

239 One can notice that all examined cases are the extreme limits of one
 equation:

$$k_L a = \frac{\dot{m} - \int C_{\text{outlet}}(t) u(L_{\text{unit}}, y) dy + \int C_{\text{inlet}}(t) u(0, y) dy}{V \Delta C}, \quad (18)$$

240 where $\Delta C = C^* - \langle C(t) \rangle$ with $\langle C(t) \rangle$ taken to be the average concentration in
 241 the whole liquid domain, \dot{m} is the mass gain in the domain, $\int C_{\text{inlet}} u(0, y) dy$
 242 and $\int C_{\text{outlet}} u(L_{\text{unit}}, y) dy$ are inlet/outlet mass fluxes. Eq. ?? describes the
 243 mass balance: whatever was generated by the bubble surface equals the
 244 domain mass change minus whatever left the domain plus whatever entered
 245 it.

Periodic boundary conditions are the extreme limiting case of Eq. ??:

$$\int C_{\text{outlet}}(t) u(L_{\text{unit}}, y) dy = \int C_{\text{inlet}}(t) u(0, y) dy.$$

246 Another limiting case (will be shown later) is when the mass accumulation
 247 rate equals zero, i.e. $\dot{m} = 0$. This situation corresponds to a simulation of a
 248 few unit cells with open boundary for flows with $Ca > 0.7$.

249 Before we examine all the test cases above, some lattice Boltzmann mass
 250 transfer benchmarks will be presented.

251 3. Validation

252 As was discussed earlier, analytical correlations for the mass transfer co-
 253 efficient have been derived for a Taylor bubble train flow as two separate
 254 contributions: the mass transfer from two half circles and the mass transfer
 255 from the film. We will examine these mass transfer cases closely with the
 256 help of the lattice Boltzmann method and compare them against analyti-
 257 cal solutions. The next sections will give a short introduction to the lattice
 258 Boltzmann method and present benchmark results.

259 3.1. TRT D2Q9 model

The lattice Boltzmann equation (LBE) operates on a square/cubic grid representing the physical domain. It utilizes probability distribution functions (also known as particle populations) containing information about macroscopic variables, such as fluid density and momentum. LBE consists of two parts: a local collision step, and a propagation step which transports information from one node to another along directions specified by a discrete velocity set. The LBE is typically implemented as follows:

$$\begin{aligned} f_i^*(\mathbf{x}, t) &= f_i(\mathbf{x}, t) - \omega(f_i(\mathbf{x}, t) - eq_i(\mathbf{x}, t)), & \text{collision step} \\ f_i(\mathbf{x} + \mathbf{c}_i, t + 1) &= f_i^*(\mathbf{x}, t), & \text{propagation step,} \end{aligned} \quad (19)$$

260 where f_i is the probability distribution function in the direction \mathbf{c}_i , eq_i is
 261 the equilibrium probability distribution function, and ω is the relaxation
 262 parameter. The term $-\omega(f_i - eq_i)$ is the so-called BGK collision operator
 263 [?]. However, the approach used here is the TRT (two-relaxation-times)
 264 collision operator [? ?]. In comparison with the widely used BGK collision
 265 operator, the TRT collision operator has better accuracy for diffusion and
 266 convection fluxes, as well as a larger range of parameters where the scheme
 267 is stable.

The TRT collision operator [?] decomposes the populations and the equilibrium distribution into a symmetric and an antisymmetric part:

$$f_i^\pm = \frac{f_i \pm f_{\bar{i}}}{2}, \quad eq_i^\pm = \frac{eq_i \pm eq_{\bar{i}}}{2}, \quad (20)$$

where \bar{i} is the opposite direction to the i -th direction. The collision is performed with two independent relaxation rates for symmetric and antisymmetric modes:

$$\begin{aligned} f_i^*(\mathbf{x}, t) &= f_i(\mathbf{x}, t) - \omega_+(f_i^+ - eq_i^+) - \omega_-(f_i^- - eq_i^-) \\ f_i(\mathbf{x} + \mathbf{c}_i, t + 1) &= f_i^*(\mathbf{x}, t). \end{aligned} \quad (21)$$

268 Note that the TRT collision operator reduces to the BGK operator if $\omega_+ =$
 269 ω_- . In comparison with the BGK collision operator, the TRT collision op-
 270 erator has one additional degree of freedom. The TRT operator introduces
 271 the following free parameter $\Lambda = \left(\frac{1}{\omega_+} - \frac{1}{2}\right)\left(\frac{1}{\omega_-} - \frac{1}{2}\right)$. This free parameter
 272 controls the effective location of bounce-back walls [?], second-order accu-
 273 racy of boundary [?] and interface schemes [?], spatial accuracy [? ?],
 274 consistency [?] and, to some extent, stability [? ? ?]. In particular, $\Lambda = \frac{1}{4}$
 275 achieves the optimal stability for the isotropic advection-diffusion equation
 276 [?].

The parameters ω_+ , ω_- and eq_i fully define the lattice Boltzmann procedure. The two-dimensional, nine-velocity LBM $D2Q9$ we used in this work is defined on the set of lattice velocities with components:

$$\begin{aligned} c_{ix} &= \{0, 1, 0, -1, 0, 1, -1, -1, 1\}, \text{ for } i = 0 \dots 8 \\ c_{iy} &= \{0, 0, 1, 0, -1, 1, 1, -1, -1\}, \text{ for } i = 0 \dots 8. \end{aligned} \quad (22)$$

The equilibrium functions for the $D2Q9$ TRT model are represented as [?]:

$$\begin{aligned} eq_i^+ &= eq_i^{(m)} + g^{(u)} eq_i^{(u)} \\ eq_i^{(m)} &= t_i^{(m)} c_e + eq_i^{(a)} \\ eq_i^{(u)} &= t_i^{(u)} \frac{u_x^2 + u_y^2}{2} + \frac{u_x^2 - u_y^2}{4} p_i^{(xx)} + g_{xy}^{(u)} \frac{u_x u_y}{4} p_i^{(xy)} \\ eq_i^{(a)} &= \frac{K_{xx} - K_{yy}}{4} p_i^{xx} + \frac{K_{xy}}{4} p_i^{(xy)} \\ eq_i^- &= t_i^{(a)} u_\alpha c_{i\alpha}, \end{aligned} \quad (23)$$

where $K_{xx,yy,xy}$ are proportional to components of the diffusion tensor, $c_e = \frac{K_{xx} + K_{yy}}{2}$, parameters $g^{(u)}$ and $g_{xy}^{(u)}$ are either zero or one (see below), the tensor $p_i^{(xx)} = c_{ix}^2 - c_{iy}^2$, the tensor $p_i^{(xy)} = c_{ix} c_{iy}$, the weights $t_i^{(u,m,a)}$ can be chosen based on stability criteria. The most commonly used set of weights, the

so-called “hydrodynamic“ weights, were chosen:

$$t_i^{(u)} = t_i^{(m)} = t_i^{(a)} = \left\{0, \frac{1}{3}, \frac{1}{3}, \frac{1}{3}, \frac{1}{3}, \frac{1}{12}, \frac{1}{12}, \frac{1}{12}, \frac{1}{12}\right\} \quad (24)$$

It can be shown through the Chapman-Enskog procedure [?], that the simple update rule with the equilibrium function presented above restores the anisotropic advection-diffusion equation:

$$\partial_t C + \partial_\alpha C u_\alpha = \partial_{\alpha\beta} D_{\alpha\beta} C, \quad (25)$$

where the concentration $C = \sum_i f_i$, and $D_{\alpha\beta} = \left(\frac{1}{\omega_-} - \frac{1}{2}\right) K_{\alpha\beta}$ is the following diffusion tensor:

$$D_{\alpha\beta} = \begin{pmatrix} D_{xx} + \left(\frac{1}{\omega_-} - \frac{1}{2}\right)(g^{(u)} - 1)u_x^2 & D_{xy} + \left(\frac{1}{\omega_-} - \frac{1}{2}\right)(g_{xy}^{(u)} - 1)u_x u_y \\ D_{xy} + \left(\frac{1}{\omega_-} - \frac{1}{2}\right)(g_{xy}^{(u)} - 1)u_x u_y & D_{yy} + \left(\frac{1}{\omega_-} - \frac{1}{2}\right)(g^{(u)} - 1)u_y^2 \end{pmatrix} \quad (26)$$

277 We want to resolve the isotropic advection-diffusion equation, $D = D_{xx} =$
 278 D_{yy} or $K = K_{xx} = K_{yy}$, with the non-diagonal diffusion tensor components
 279 set to zero ($D_{xy} = 0$). In contrast to the $D2Q5$ model, with $D2Q9$ it is possi-
 280 ble to cancel the numerical diffusion by the proper choice of the equilibrium
 281 functions, i.e. $g_{xy}^{(u)} = g^{(u)} = 1$. The particular choice of parameters used in
 282 simulations is $c_e = \frac{1}{3}$, $\Lambda = \frac{1}{4}$. Thus, the diffusion coefficient D is matched
 283 through ω_- , i.e. $D = c_e \left(\frac{1}{\omega_-} - \frac{1}{2}\right) = \frac{1}{3} \left(\frac{1}{\omega_-} - \frac{1}{2}\right)$. For the particular choice
 284 $\Lambda = \frac{1}{4}$, ω_+ can be found easily as $\omega_+ = 2 - \omega_-$.

We validated two types of boundary conditions: Inamuro boundary conditions [?] and pressure anti bounce-back boundary conditions [?]. However, the simulation results are presented only for pressure anti bounce-back due to their ability to handle complex boundaries in a simple way:

$$f_{B,i}^* = -f_{F,\bar{i}}^* + 2eq^+(C^*, \mathbf{u}), \quad (27)$$

285 where C^* is the concentration to be imposed at the surface, \mathbf{u} is the surface
 286 velocity, i is the direction number pointing to the domain located at the
 287 boundary surface B , \bar{i} is the direction number opposite to i and is located at
 288 the fluid node F specifically so that node B is located at the location $F + \mathbf{c}_i$.

289 Note that the parameters of the lattice Boltzmann scheme are connected
 290 with physical parameters only through non-dimensional numbers governing

the physics of the problem. In our case, this number is the Peclet number, $Pe = \frac{U_{\text{bubble}} L}{D}$. Therefore, one can choose any quantity, for example U_{bubble} in the lattice Boltzmann units as long as the Peclet number is matched in physical space and numerical simulations. The fact that U_{bubble} can be varied in certain ranges is extremely useful in the context of numerical simulations. This allows to increase the time step and decrease the computational demand (by an order of magnitude). This point will be used in simulations and covered later.

The next section will cover LBM benchmarks that resemble the mass transfer from a bubble (mass transfer to the liquid with the parabolic velocity profile and mass transfer from a cylinder).

3.2. The radial case

The case to be examined is the mass transfer from a circle with radius a , with the circle approximated as a stair-case. It can be described by the following system of equations:

$$\begin{aligned}\partial_t C(r, t) &= \frac{1}{r} \partial_r r \partial_r C(r, t) \\ C(a, t) &= C_0, \quad C(r, 0) = C_{\text{init}}\end{aligned}\tag{28}$$

The analytical solution is [?]:

$$\frac{C(r, t) - C_0}{C_{\text{init}} - C_0} = \sum_{n=1}^{\infty} \frac{2}{\mu_n J_1(\mu_n)} \exp\left(-\mu_n^2 \frac{Dt}{a^2}\right) J_0\left(\mu_n \frac{r}{a}\right),\tag{29}$$

where μ_n is the n -th zero root of the 0th order Bessel polynomial $J_0(\mu_n) = 0$. Some of the corresponding roots are as follows: $\mu_1 = 2.4048$, $\mu_2 = 5.5201$, $\mu_3 = 8.6537$, $\mu_4 = 11.7915$, $\mu_5 = 14.9309$. By taking the initial concentration as 0, one obtains:

$$C(r, t) = C_0 \left(1 - \sum_{n=1}^{\infty} \frac{2}{\mu_n J_1(\mu_n)} \exp\left(-\mu_n^2 \frac{Dt}{a^2}\right) J_0\left(\mu_n \frac{r}{a}\right) \right).\tag{30}$$

The solution depends only on the non-dimensional time: $\tau = \frac{Dt}{a^2}$. The domain size was 129×129 with the circle radius $a = 40$ lattice units. Some results for different diffusion coefficients are presented in Fig.???. The numerical simulations with the bounce-back boundary conditions are able to accurately reproduce the analytical results.

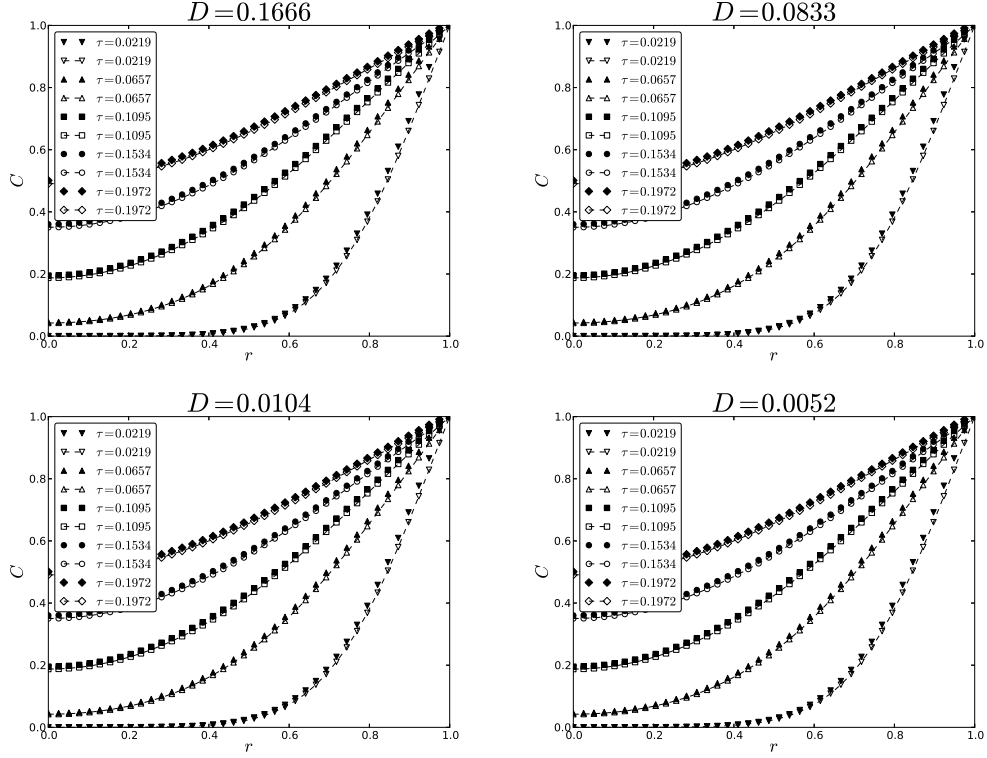


Figure 5: Profiles for different diffusion parameters varied with ω_- (lines: Eq. ??, symbols: LB results). One can see that the diffusion from curved boundaries is captured accurately . r is the distance from the center.

3.3. Poiseuille velocity profile

The problem we want to address can be formulated through the following PDE:

$$\begin{aligned}
 \frac{\partial C}{\partial x} U(y) &= D \frac{\partial^2 C}{\partial y^2} \\
 C(0, y) &= 0, \quad C(x, \pm\delta) = C^*, \quad \frac{\partial C}{\partial y}(x, 0) = 0 \\
 U(y) &= U_0 \left(1 - \left(\frac{y}{\delta} \right)^2 \right)
 \end{aligned} \tag{31}$$

The procedure to solve this problem is presented in Appendix ?? which yields the final solution as:

$$C = C^* - C^* \sum_{m=0} C_m e^{-m^4 \frac{x}{\delta} \frac{1}{Pe}} e^{-m^2 y^2 / (2\delta^2)} {}_1F_1\left(-\frac{m^2}{4} + \frac{1}{4}, \frac{1}{2}, m^2 \frac{y^2}{\delta^2}\right), \quad (32)$$

where coefficients C_m are taken from Eq. ?. The comparison between contours of analytical and simulation results is presented in Fig. ?. Parameters were taken as: $D = 0.0185$, the grid dimension is 80×1600 . The centerline velocity is $U_0 = 0.05$ which yields the Peclet number $Pe = U_0 \delta / D = 108.108$. The results are in good agreement. The simulations capture accurately the singular derivative for $x = 0$.

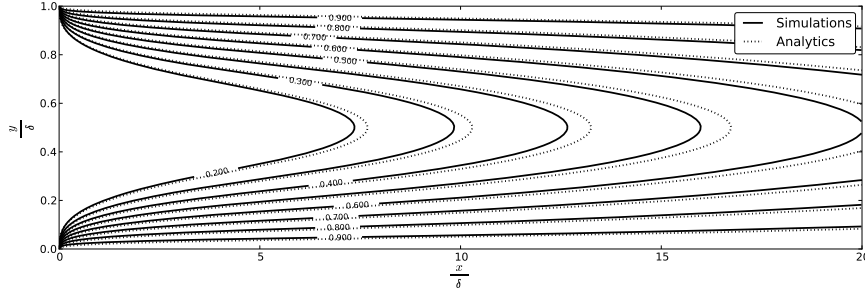


Figure 6: Comparison between the analytical concentration contours and simulations with pressure anti bounce-back conditions, Eq. ?. The simulation was done for $D = 0.0185$ with a 80×1600 grid. The centerline velocity is $U_0 = 0.05$, and the Peclet number is 108.108.

Now the LBM is validated against the benchmarks relevant for the flow around bubbles, one can examine the cases mentioned in Section ?? to calculate the volumetric mass transfer coefficient for Taylor bubble train flow.

4. Numerical approach

A multiphase code was utilized to obtain the flow patterns and bubble shapes for different capillary numbers [?]. Five particular cases were chosen to be examined, their results are summarized in Table ?. Note that the velocities (LB system) in Table ?? are small. This means that to match large Peclet numbers, $Pe = \frac{U_{\text{bubble}} L}{D}$, usually used in experiments, one needs

Ca	Re	U_{bubble}	δ	ε_{gas}	U_{liq}	U_{gas}	L_{bubble}	L_{slug}
0.097	1.656	0.0055	0.092	0.30	0.0046	0.0016	5.79	9.21
0.254	4.318	0.0143	0.132	0.28	0.0108	0.0041	6.12	8.88
0.526	8.938	0.0297	0.157	0.27	0.0209	0.0080	6.19	8.81
0.750	12.744	0.0424	0.167	0.25	0.0293	0.0107	5.96	9.04
1.040	17.665	0.0588	0.177	0.22	0.0397	0.0135	5.59	9.41

Table 1: Sample results with the binary liquid lattice Boltzmann model [?]. The following notations are used: the capillary number $Ca = \frac{U_{\text{bubble}}L}{\rho\nu_{\text{liq}}}$, U_{liq} is the superficial liquid velocity, U_{gas} is the superficial gas velocity. δ is the non-dimensional film thickness, L_{bubble} and L_{slug} are the non-dimensional bubble and slug lengths (defined in channel heights). The simulation sketch is presented in Fig. ??.

to decrease the diffusion coefficient $D = \frac{1}{3}\left(\frac{1}{\omega_-} - \frac{1}{2}\right)$. Thus, the parameter $\omega_- \approx 0.5$. However, for such values of ω_- the stability of the lattice Boltzmann method drastically decreases [?]. On the other hand, one iteration in the lattice Boltzmann system corresponds to a physical time step $\Delta t = U_{\text{bubble,LB}} \frac{\Delta x}{U_{\text{bubble,phys}}}$. The iteration time is proportional to the velocity U_{LB} and the typical number of simulation steps to obtain the steady-state mass transfer coefficient for $Ca < 0.2$ is of the order of a few million. Therefore, it is desirable to increase U_{LB} while maintaining the Peclet number. If one increases the velocity, then ω_- increases as well, which impacts positively on the stability of the LBM.

Given all the considerations above, mass transfer simulations are performed as follows:

Flow field Given a capillary number Ca , one needs to obtain hydrodynamic fields around the bubble using the multiphase binary liquid lattice Boltzmann model according to our previous work [?]. Periodic boundary conditions were used in that work. The grid used was 202×3000 which corresponds to the fluid domain of size 200×3000 . That grid resolution was taken to ensure grid independency of the results [?]. Note that we do not approximate bubble shapes by correlations, but we directly resolve them by using the multiphase solver.

Bubble reference frame Once the hydrodynamics is solved, the mass transfer simulations are conducted in the reference frame moving with the bubble, where the bubble stands still and the liquid flows around the bubble. We impose a uniform and steady concentration on the surface

348 of the bubble with the anti bounce-back condition, Eq. ??.

349 **Velocity improvement** One can scale the velocity to perform faster sim-
 350 ulations. However, before doing it one needs to improve the velocity
 351 field. This issue arises because of the multiphase model used in the
 352 flow simulations. The binary liquid lattice Boltzmann model is a dif-
 353 fuse interface model where no clear boundary between gas and liquid
 354 exists. We obtain the bubble shape by imposing a condition on the
 355 order parameter field ϕ with $\phi \leq 0$ in the bubble [?]. The velocity of
 356 the bubble is defined as the bubble tip velocity. Because of the square
 357 grid, the shape of the bubble is determined within an accuracy of one
 358 grid spacing. Thus, there is an error in the determination of the bubble
 359 velocity. Though these errors are small, there is still a small non-zero
 360 velocity component pointing into the bubble in some places, see Fig.
 361 8 in [?] where some streamlines are penetrating the bubble surface.
 362 This small velocity is amplified upon the velocity scaling and is incon-
 363 sistent with the advection-diffusion equation leading to instability after
 364 many iterations.

365 Thus, before performing the mass transfer simulations an additional
 366 single phase hydrodynamic simulation is performed. A free-surface
 367 solver was developed in order to obtain a velocity field consistent with
 368 the advection-diffusion equation. We take results from the multiphase
 369 simulations, extract a bubble shape using the phase indicator $\phi \leq 0$,
 370 and approximate the bubble shape by the stair-case line with imposed
 371 free-slip boundary condition on it. The obtained bubble velocity is
 372 then imposed on the walls. This corresponds to conducting simulations
 373 in the reference frame moving with the bubble. Appendix ?? covers
 374 the simple free-slip boundary condition implementation drastically im-
 375 proving velocity patterns. The system is iterated until a steady state
 376 is reached. Note, that these type of simulations are much faster than
 377 the original multiphase simulations. As the output all the non-zero ve-
 378 locity components perpendicular to the bubble surface are completely
 379 eliminated. We compared original multiphase simulations with one-
 380 component free-slip simulations. All quantities such as superficial slug
 381 and liquid velocities are within 3% for the capillary number in the range
 382 $0.05 \leq Ca \leq 1.0$. One can see in Fig. ?? two streamline profiles for
 383 $Ca = 0.097$ and $Ca = 1.040$.

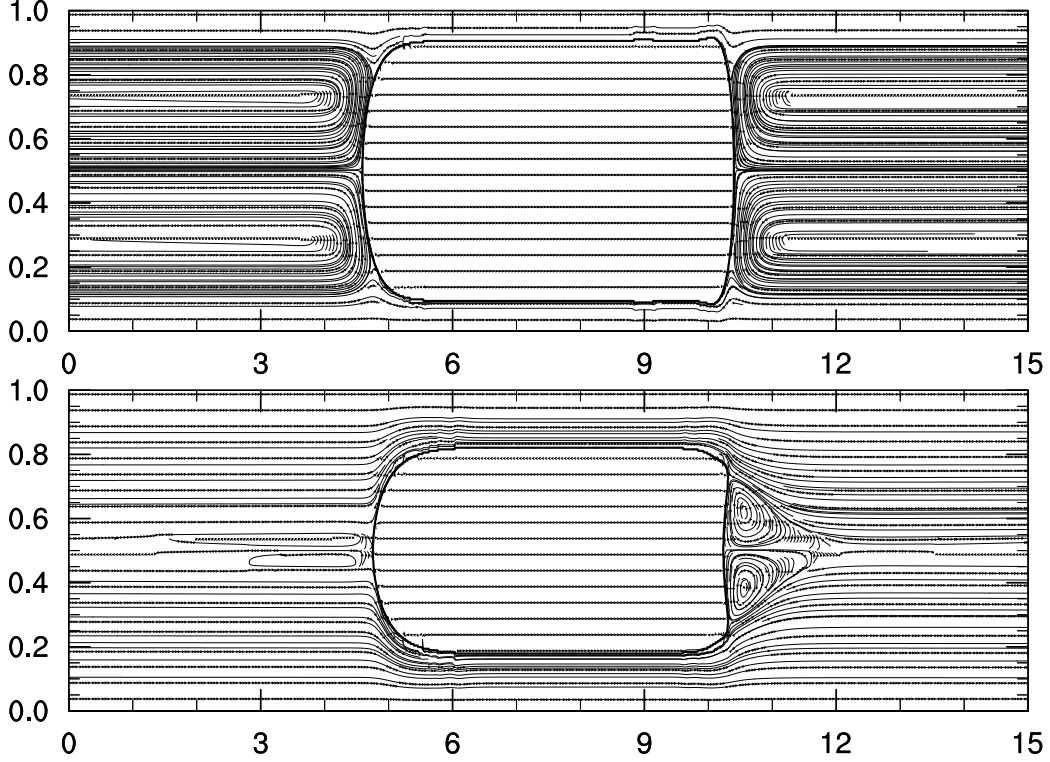


Figure 7: The streamline patterns produced by the free-surface flow solver with simplified approximation of the free-slip bubble surface, see Appendix ???. Two completely different velocity patterns are obtained, $Ca = 0.097$ (top) and $Ca = 1.040$ (bottom).

384 **Mass transfer** After improved velocity profiles are obtained one can per-
 385 form any mass transfer simulations with the various boundary condi-
 386 tions as covered in Section ??. For this purpose one needs to match
 387 the Peclet number Pe taken from experiments.

388 5. Results

389 This section covers simulation results. We first examine the possibility
 390 to increase the fluid velocity while keeping the Peclet number the same.
 391 After that the results for periodic boundary conditions for 5 capillary number
 392 cases will be presented. Finally, we will examine many cell simulations for
 393 two representative velocity patterns related to $Ca = 0.0907$ and $Ca = 1.04$
 394 respectively (see Fig. ??).

395 5.1. Velocity scaling at constant Peclet number

This section addresses the process of significantly increasing the velocity magnitude while keeping dimensionless parameters the same to speed up simulations. This is especially important to be able to simulate a few unit cells in a reasonable time. For example, ten unit cell simulations require a grid of 30000×202 nodes. Since the Peclet number is the only dimensionless quantity governing the advection-diffusion equation:

$$Pe = \frac{U_{\text{bubble}} N_y}{D}. \quad (33)$$

396 one needs to increase the diffusion coefficient when the velocity is increased.
 397 Simulation runs were made with velocities 2, 4, 6, 8, 10, 15, 20, 40 times larger
 398 than the original velocities. The velocities and their corresponding capillary
 399 numbers are presented in Table ???. Periodic boundary conditions were used
 400 and the mass transfer coefficient was calculated according to Eq. 4. Table
 401 ??? shows that the velocity limit for periodic boundary conditions is 0.1, so
 402 to be on the safe side, velocities should not be scaled up beyond that value.
 403 For example, in Table ?? for small capillary numbers ($Ca < 0.2$) one can
 404 scale up velocity significantly (20 – 40 times) to obtain a velocity around
 405 0.2 where simulations are still stable. However, for larger capillary numbers
 406 the scale up is smaller (2 – 4 times), and the velocity for stable simulations
 407 is smaller than 0.1 . It gives us a preliminary idea to what extent one can
 408 scale periodic mass transfer simulations. The concentration contour profiles
 409 corresponding to Table ?? for different velocity scalings are presented in Fig.
 410 ??. One can see an acceptable agreement between the cases with the same
 411 Peclet number but different velocity scalings. Note, that the speedup can be
 412 up to 10 to 40 times.

413 5.2. Average concentration results

414 In this section we will examine the case where the volume averaged con-
 415 centration over time is used as the characteristic concentration. To calculate
 416 the volumetric mass transfer coefficient we used Eq. ??. Results for the
 417 coefficient $k_L a \frac{U_{\text{bubble}}}{U_{\text{gas}} + U_{\text{liq}}}$ are shown in Fig. ?? for different Peclet numbers and
 418 velocity scalings indicated in Table ??. When the average concentration gets
 419 close to $C^* = 1$ then Eq. ?? gives inadequate results due to accuracy of
 420 the logarithmic function evaluation. This is the reason that curves in Fig.
 421 ?? tend to shoot up for long times. Due to velocity scaling each simula-
 422 tion has a different physical time step. Thus, we normalized time such that

Scale	U_{bubble}	ω_-	Time Iterations	C_{aver}
-------	--------------	------------	-----------------	------------

$$Ca = 0.097, Pe = 1313$$

2	0.011	1.98	400000	0.318
4	0.023	1.96	200000	0.319
8	0.044	1.92	100000	0.320
10	0.055	1.90	80000	0.321
20	0.11	1.81	40000	0.324
40	0.22	1.66	20000	0.328

$$Ca = 0.254, Pe = 3414$$

2	0.0286	1.98	800000	0.6533
4	0.0572	1.96	400000	0.6591
8	0.1144	1.92	200000	0.6692
10	0.1430	1.90	160000	0.6734
20	0.2860	1.81	80000	0.6894

$$Ca = 0.526, Pe = 7092$$

2	0.0594	1.98	200000	0.3271
4	0.1188	1.96	100000	0.3315

$$Ca = 0.750, Pe = 10125$$

2	0.0848	1.98	200000	0.3489
---	--------	------	--------	--------

$$Ca = 1.040, Pe = 14041$$

2	0.1176	1.98	200000	0.3675
---	--------	------	--------	--------

Table 2: Indications of the achievable stable velocity U_{bubble} when one scales velocity. Since the physical time step represented by a single iteration of the simulation is directly proportional $U_{bubble, LB}$, scaling the velocity directly translates to an effective speed-up of the simulation. Note that time iterations indicated in the table correspond to the same moment in physical time. One can see that scaling produces adequate results when C_{aver} is compared. The contour profiles for all of these cases (capillary number Ca and all scales) are presented in Fig. ??.

423 it represents a number of unit cell lengths which the bubble will pass, i.e.
424 $N_{cell\ units} = \frac{scale \cdot U_{bubble} \cdot N_{iter}}{L_{unit}}$. Fig. ?? shows the volumetric mass transfer de-

pendency against the distance in unit cell length. One can see in Table ?? that for different Peclet numbers different time (number of unit cells) is required to achieve steady state. For example, for larger Peclet numbers fewer iterations are required to achieve the steady state condition.

Overall one obtains steady state volumetric mass transfer coefficients for periodic boundaries simulations if the following conditions are fulfilled:

- I Scaling is performed as $U_{max} = \text{scale} \cdot U_{\text{bubble}} \leq 0.1$.
- II The larger the Peclet number, the fewer iterations are required. One can extrapolate data from Table ??, say L_{steady} , and estimate the number of iterations to reach the steady-state as $\text{scale} \cdot U_{\text{bubble}} \cdot N_{\text{iter}} \leq L_{\text{steady}}$.

Ca	Pe	$L_{\text{steady}}/L_{\text{unit}}$	$k_L a \frac{L_{\text{unit}}}{U_{\text{bubble}} + U_{\text{gas}}}$
0.097	1313	7	0.21
0.254	3414	6	0.14
0.526	7092	3	0.095
0.750	10125	3	0.074
1.040	14041	2	0.0601

Table 3: The distance which a bubble propagates when the steady-state condition is achieved.

5.3. Periodic boundaries with the inlet/outlet characteristic concentration

The volumetric mass transfer coefficient was calculated using Eq. ?? with the characteristic concentration being the inlet/outlet flux averaged concentration as used by ?]. One can see in Fig. ?? that the calculated volumetric mass transfer behave differently from the domain averaged volumetric mass transfer coefficient. For example, for small capillary numbers, i.e. $Ca = 0.097, 0.254, 0.526$ the values are overpredicted ($k_L a \frac{L_{\text{unit}}}{U_{\text{bubble}} + U_{\text{gas}}} = 0.3, 0.25, 0.1$). When the velocity pattern changes from having a vortex in front of the bubble to not having it, i.e. $Ca = 0.75, 1.04$ the calculated values are underpredicted compared to estimates based on volume-averaged concentration, i.e. $k_L a \frac{L_{\text{unit}}}{U_{\text{bubble}} + U_{\text{gas}}} = 0.06, 0.04$. As we will see later, the domain-averaged characteristic concentration produces proper mass transfer coefficients.

448 5.4. *Van Baten and Krishna formulation*

449 The Δt formulation, Eq. ??, is calculated as the change of mass in the
 450 domain divided by the time difference. We examined two approaches: the
 451 characteristic concentration taken to be as the domain average and as the
 452 flux-averaged input/output concentration. The latter case corresponds to [?
 453]. The results are presented in Fig. ?? for $Ca = 0.097$ and $Ca = 1.04$. One
 454 can see that the inlet/outlet flux averaged concentration is inconsistent. The
 455 reason that [?] obtained the mass transfer coefficient close to the analytical
 456 estimation is that the liquid slug is well mixed ($Ca < 0.1$ which is below
 457 the range studied here) so that the averaged concentration is close to the
 458 inlet/outlet concentration.

459 However, results for the domain-averaged concentration using the ap-
 460 proach of [?] are close to simulation results in Section ???. Note that for
 461 $Ca = 0.097$ the obtained mass transfer coefficient value is 10% lower than
 462 the value in Section ???. However, as will be shown later the obtained volu-
 463 metric mass transfer coefficient for $Ca = 0.0097$ has the same value as for the
 464 simulations of a few unit cells. Therefore the approach of [?] produces ac-
 465 curate results but if the characteristic concentration is the volume-averaged
 466 concentration (not the inlet/outlet flux-averaged concentration used in the
 467 original work). From the computational point of view, it also requires the
 468 concentration fields in time and space to calculate the mass change in time
 469 and the averaged domain characteristic concentration.

470 5.5. *Simulations for several unit cells*

471 In order to achieve independence from the boundary conditions and a
 472 closer match with the physical system being modelled, one can simulate
 473 several unit cells, corresponding to a head of the bubble train. If end effects
 474 are eliminated then the average domain characteristic should change in time
 475 according to Eq. ???. This eliminates the ambiguity inherent in choosing a
 476 definition of the characteristic concentration, it becomes the same domain-
 477 averaged concentration as the one measured in experiments.

478 This section studies the number of unit cells required for the volumetric
 479 mass transfer coefficient to be independent of the influence of boundaries.
 480 We chose two different velocity patterns (see Fig. ?? for $Ca = 0.097$ and
 481 $Ca = 1.04$) to perform the simulations. For $Ca = 0.097$ we performed
 482 simulations with 4, 6, 8, 10 cells, and for $Ca = 1.040$ only with 4, 6, 8 cells.
 483 We observed however that simulations with a domain length of 10 unit cells
 484 produce the same results as those with 8 unit cells.

485 We keep velocity in the range $0.05 - 0.1$ to avoid excessively long simula-
 486 tion times. The number of steps for mass to pass through the whole domain
 487 can be approximated as $1.5 \frac{L_{\text{unit}}}{U_{\text{bubble}}}$, which takes into account the bulk veloc-
 488 ity. If U_{bubble} is taken as 0.05 then for the domain size $L_{\text{unit}} = 3000$ one can
 489 obtain the following number of iterations for the mass to cross the unit cell
 490 $1.5 \frac{3000}{0.05} = 90000$. Therefore, 10^6 iterations are enough for a system consisting
 491 of 10 unit cells. For more accurate estimations of the number of time steps
 492 depending on the Peclet number we refer to Section ??.

493 5.6. $Ca = 0.097$ results

There are two characteristics we want to track in the simulations: the
 average concentration in the unit cell with time (see Eq. ??), and the accu-
 mulated mass rate in the domain which takes into the account inlet/outlet
 fluxes (see Eq. ??). The former resembles experiments: if one has a large
 enough number of unit cells, then the averaged domain concentration should
 change in time according to Eq. ??:

$$k_L a \frac{L_{\text{unit}}}{U_{\text{gas}} + U_{\text{liq}}} = \frac{L_{\text{unit}}}{U_{\text{bubble}}(t_2 - t_1)} \ln \left(\frac{C^* - \langle C(t_1) \rangle}{C^* - \langle C(t_2) \rangle} \right) \quad (34)$$

494 The non-dimensional volumetric mass transfer coefficient calculated based
 495 on Eq. ?? (domain-averaged concentration change in time) is represented
 496 in Fig. ?? for different unit cells. One can see that mass transfer coeffi-
 497 cient values are the same as the mass flux concentration based on the ?
 498 formulation with the characteristic concentration being the domain-averaged
 499 concentration (see Section ??). This demonstrates two things: the domain-
 500 averaged concentration is the only choice for the characteristic concentration,
 501 and periodic boundary conditions for one unit cell produce good results.

In comparison with periodic boundary conditions Eq. ?? allows to calcu-
 late the mass transfer coefficient differently. Eq. ?? can be rewritten as:

$$k_L a \frac{L_{\text{unit}}}{U_{\text{bubble}} + U_{\text{gas}}} = \frac{L_{\text{unit}}}{U_{\text{gas}} + U_{\text{bubble}}} \frac{V \frac{\langle C(t_2) \rangle - \langle C(t_1) \rangle}{t_2 - t_1}}{- \int C_{\text{outlet}}(L_{\text{unit}}, y, t^*) u(L_{\text{unit}}, y) dy + \int C_{\text{inlet}}(0, y, t^*) u(0, y) dy \over V(C^* - \langle C(t^*) \rangle)}, \quad (35)$$

502 where t^* is the mean between t_1 and t_2 .

503 Fig. ?? shows average concentrations in different units and $k_L a \frac{L_{\text{unit}}}{U_{\text{bubble}} + U_{\text{gas}}}$
 504 based on Eq. ?? calculated for each unit for velocity scale 10 and 6 unit cells

(all velocity scales produce the same results). It shows that the volumetric mass transfer coefficient is consistent for internal segments, i.e. unit cells numbers 2 – 4. The results for the volumetric mass transfer coefficient calculated by Eq. ?? for multiple unit cells are close (less than 10% deviation) to results for periodic boundary conditions in Section ?? . The same dependencies can be found for 8 and 10 unit cells simulations but we do not present them here. We also do not present 4 units cells simulation results which are highly influenced by entrance and exit effects.

The calculation of the volumetric mass transfer coefficient is more difficult using Eq. ?. However, it will be shown below that this equation can be significantly simplified in case of larger capillary numbers ($Ca > 0.7$).

5.7. $Ca = 1.040$ results

The same correlations were examined for a different velocity pattern at $Ca = 1.040$. The original Peclet number we started with is $Pe = 14041$ (Table ??). To improve stability we changed the original Peclet number by increasing diffusion to $Pe = 2644$. The results with respect to the number of unit cells are the same as for $Ca = 0.097$: at least 6 unit cells are required to avoid the influence of inlet/outlet effects. Thus, only 6 unit cells results are presented in Fig. ?? which shows the average concentration for each unit cell. One can see that the average volume concentration for each unit cell converges to a constant value. Thus, all the mass generated by the bubble is transferred through the boundaries. This indicates that the liquid slug is unmixed since no concentration travels back to inlet with the vortex and increases the average concentration in each unit cell. Note that the periodic boundary conditions cannot show whether the liquid slug is mixed or not due to the fact that the averaged domain concentration always increases in time. Thus, the volumetric mass transfer coefficient $k_L a \frac{L_{\text{unit}}}{U_{\text{bubble}} + U_{\text{gas}}}$ can be calculated according to the definition, Eq. ??:

$$k_L a = \frac{\dot{m} - \int C_{\text{outlet}}(y)u(L_{\text{unit}}, y)dy + \int C_{\text{inlet}}(y)u(L_{\text{unit}}, y)dy}{V(C^* - \langle C(t) \rangle)}, \quad (36)$$

where V is the unit cell volume. There is no accumulated mass in the domain, so $\dot{m} = 0$. Like periodic boundary conditions, this case is another extreme limit of Eq. ?. Note that to calculate the volumetric mass transfer coefficient one needs only the spatial information and does not require the

521 knowledge of how the averaged concentration changes in time, which signifi-
 522 cantly lowers storage requirements for the simulations with $Ca > 0.7$ where
 523 there is no vortex in the liquid slug.

524 Fig. ?? (bottom) shows the volumetric mass transfer coefficient based
 525 on spatial calculations of inlet/outlet concentrations. One can see that the
 526 volumetric mass transfer coefficient is close to the calculated volumetric mass
 527 transfer coefficient using the time averaged approach and periodic boundaries
 528 one unit cell simulations (presented in the same figure for comparison). Note
 529 that results for approaches which incorporate the volume-averaged character-
 530 istic concentration either for one cell or a few unit cells coincide. Therefore,
 531 for certain hydrodynamic patterns ($Ca > 0.7$), one can easily convert time
 532 domain to spatial domain calculations using simulations of several unit cells.

534 5.8. Comparison of experimental and analytical correlations

While the goal of this paper is not to compare simulation results with the
 experimental measurements, we felt that a short note about such comparison
 will be beneficial. Unfortunately, to the authors' knowledge, there are no
 reported experimental results measuring the mass flux for bubbles flowing
 between parallel plates. However, an interesting correlation for the mass
 transfer volumetric coefficient was presented by [?] for three-dimensional
 microchannel geometries:

$$k_L a = \frac{2}{d_h} \left(\frac{DU_{\text{bubble}}}{L_{\text{bubble}} + L_{\text{slug}}} \right)^{0.5} \left(\frac{L_{\text{bubble}}}{L_{\text{bubble}} + L_{\text{slug}}} \right)^{0.3}$$

$$k_L a \frac{L_{\text{unit}}}{U_{\text{gas}} + U_{\text{liq}}} = 2 \frac{L_{\text{unit}}}{d_h} \left(\frac{D}{L_{\text{unit}}(U_{\text{bubble}} + U_{\text{gas}})} \frac{U_{\text{bubble}}}{U_{\text{gas}} + U_{\text{liq}}} \right)^{0.5} \left(\frac{L_{\text{bubble}}}{L_{\text{bubble}} + L_{\text{slug}}} \right)^{0.3} \propto Pe^{-\frac{1}{2}} \quad (37)$$

One can see that the volumetric mass transfer correlation should be approx-
 imately proportional to $Pe^{-0.5}$. One can also use analytical estimates of the
 volumetric mass transfer coefficient calculated using the Higbie penetration
 theory [?]. One can derive the analytical expression for the mass transfer
 for bubble train flow between parallel plates by following the works [? ?]:

$$k_L a \frac{L_{\text{unit}}}{U_{\text{bubble}} + U_{\text{gas}}} = \frac{L_{\text{unit}}}{U_{\text{gas}} + U_{\text{liq}}} \left(4 \sqrt{DU_{\text{bubble}}} \pi \frac{\sqrt{L_{\text{bubble}} - H(1 - 2\delta)}}{L_{\text{unit}} H} \right. \\ \left. + 2\sqrt{2} \sqrt{DU_{\text{bubble}}} \frac{\sqrt{H(1 - 2\delta)}}{L_{\text{unit}} H} \right), \quad (38)$$

535 where H is the channel height, and δ is the non-dimensional film thickness
 536 (in channel heights).

537 Fig. ?? shows a comparison between the correlation by ?], the ana-
 538 lytical expression, Eq. ??, and the current simulation results presented in
 539 Table ?. The coefficients are close to each other, especially given that the
 540 correlation by ?] is for three-dimensional cases. The fitting procedure for
 541 this work results showed that the power of the Peclet number dependence is
 542 -0.50038 which is close to the theoretical value -0.5 . The fitting curve is
 543 $7.745Pe^{-0.50038}$.

544 6. Summary

545 This work examines a way to calculate the volumetric mass transfer coef-
 546 ficient of Taylor/Batchelor bubble train flow in the framework of the lattice
 547 Boltzmann method. Overall, the easiest recipe is to perform simulations with
 548 periodic boundary conditions and calculate the volumetric mass transfer coef-
 549 ficient based on the domain-averaged concentration through any formulation
 550 (? , periodic boundary conditions, simulations of several unit cells) as they
 551 produce consistent results. The best accuracy is achieved with formulations
 552 based on the mass difference or on the averaged domain concentrations taken
 553 in different times, Eq. ?. Eq. ? gives a slightly overestimated volumetric
 554 mass transfer coefficients (less than 10%). The original formulation of ?]
 555 is inconsistent if one takes the inlet/outlet flux-averaged concentration to be
 556 the characteristic concentration. Simulations of several unit cells are harder
 557 to perform, but they indicate how well the liquid slug is mixed. For velocity
 558 patterns related to $Ca \geq 0.7$ simulations with a few unit cells allow to cal-
 559 culate the volumetric mass transfer coefficient based on the spatial location
 560 only, without requiring the time snapshots of domain concentration values
 561 used in all other approaches. Finally, a sample of results was compared with
 562 the experimental correlation of ?] and shown to be consistent.

563 7. Acknowledgements

564 M.J. acknowledges a scholarship from the TWING project co-financed
 565 by the European Social Fund. A.K. wants to thank Schlumberger for their
 566 financial support.

567 Appendix A. Mass transfer for planar Poiseuille flow

Close to the previous example but with a different velocity profile, the problem can be formulated through the following PDE:

$$\begin{aligned}\frac{\partial C}{\partial x} U(y) &= D \frac{\partial^2 C}{\partial y^2} \\ C(0, y) &= 0, \quad C(x, \pm\delta) = C^*, \quad \frac{\partial C}{\partial y}(x, 0) = 0 \\ U(y) &= U_0 \left(1 - \left(\frac{y}{\delta}\right)^2\right)\end{aligned}\tag{A.1}$$

The following substitution simplifies the form of equations:

$$\begin{aligned}\zeta &= \frac{x}{\delta} \frac{D}{U_0 \delta} = \frac{1}{Pe} \frac{x}{\delta} \\ \xi &= \frac{y}{\delta}.\end{aligned}\tag{A.2}$$

Then the following equation can be obtained:

$$\begin{aligned}\frac{\partial \Theta}{\partial \zeta} (1 - \xi^2) &= \frac{\partial^2 \Theta}{\partial \xi^2} \\ \Theta(\zeta, \xi) &= C - C^* \quad \Theta(0, \xi) = -C^* \quad \Theta(0, \pm 1) = 0\end{aligned}\tag{A.3}$$

After separation of variables, $\Theta(\zeta, \xi) = X(\zeta)Y(\xi)$ one can come up with two equations:

$$\begin{aligned}\frac{dX(\zeta)}{d\zeta} + m^4 X(\zeta) &= 0 \\ \frac{d^2 Y(\xi)}{d\xi^2} + m^4 (1 - \xi^2) Y(\xi) &= 0\end{aligned}\tag{A.4}$$

The first equation has a solution:

$$X(\zeta) = \exp(-m^4 \zeta)\tag{A.5}$$

The second equation can be simplified after substitution $\bar{\xi} = m\sqrt{2}\xi$ to the standard equation:

$$Y'' - \left(\frac{1}{4}\bar{\xi}^2 + a\right)Y = 0,\tag{A.6}$$

where $Y' = dY/d\bar{\xi}$, and $a = -m^2/2$. The equation above has two solutions via parabolic cylinder functions or through the confluent hypergeometric function [?]:

$$\begin{aligned} Y_1 &= e^{-\bar{\xi}^2/4} {}_1F_1\left(\frac{a}{2} + \frac{1}{4}, \frac{1}{2}, \frac{\bar{\xi}^2}{2}\right) \\ Y_2 &= e^{-\bar{\xi}^2/4} {}_1F_1\left(\frac{a}{2} + \frac{3}{4}, \frac{3}{2}, \frac{\bar{\xi}^2}{2}\right) \end{aligned} \quad (\text{A.7})$$

Taking symmetry conditions into consideration by leaving only the even solution, Eq. ?? has the following solution:

$$Y_m = C_m e^{-m^2 \xi^2/2} {}_1F_1\left(-\frac{m^2}{4} + \frac{1}{4}, \frac{1}{2}, m^2 \xi^2\right) \quad (\text{A.8})$$

To satisfy the boundary condition we need to find zeros of the hypergeometric function, i.e. ${}_1F_1\left(-\frac{m^2}{4} + \frac{1}{4}, \frac{1}{2}, m^2\right) = 0$. First ten eigenvalues can be found using numerical methods: 1.2967, 2.3811, 3.1093, 3.6969, 4.2032, 4.6548, 5.0662, 5.4467, 5.8023, 6.1373. One needs to satisfy one more condition to obtain coefficients C_m :

$$-C^* = \sum_m C_m e^{-m^2 \xi^2/2} {}_1F_1\left(-\frac{m^2}{4} + \frac{1}{4}, \frac{1}{2}, m^2 \xi^2\right) \quad (\text{A.9})$$

One can multiply both parts on $(1 - \xi^2) {}_1F_1\left(-\frac{m^2}{4} + \frac{1}{4}, \frac{1}{2}, m^2 \xi^2\right)$ and through orthogonality (Stourm-Liouville theorem) obtain coefficients:

$$C_m = -C^* \frac{\int_{\xi=0}^1 (1 - x^2) e^{-m^2 \xi^2/2} {}_1F_1\left(-\frac{m^2}{4} + \frac{1}{4}, \frac{1}{2}, m^2 \xi^2\right) d\xi}{\int_{\xi=0}^1 (1 - \xi^2) e^{-m^2 \xi^2/2} {}_1F_1\left(-\frac{m^2}{4} + \frac{1}{4}, \frac{1}{2}, m^2 \xi^2\right)^2 d\xi} \quad (\text{A.10})$$

Therefore the complete solution can be written as:

$$C = C^* - C^* \sum_{m=0} C_m e^{-m^4 \frac{x}{\delta} \frac{1}{Pe}} e^{-m^2 y^2/(2\delta^2)} {}_1F_1\left(-\frac{m^2}{4} + \frac{1}{4}, \frac{1}{2}, m^2 \frac{y^2}{\delta^2}\right), \quad (\text{A.11})$$

568 where coefficients C_m are taken from Eq. ?. For the case C^* , the first ten
569 coefficients are: 1.2008, -0.2991 , 0.1608 , -0.1074 , 0.0796 , -0.0627 , 0.0515 ,
570 -0.0435 , 0.0375 , -0.0329 .

571 Appendix B. Free surface boundary conditions

572 There are a few implementations of free boundary conditions [? ?].
573 However, we developed the easy solver to impose the free surface boundary
574 conditions at the complicated surface of the bubble. The reason is to impose
575 the symmetric boundary conditions. Because the boundary is a staircase
576 approximation, one can find the normal to the boundary which is always
577 located by the angle of multiple of 45 degrees, see Fig. ?? . This can be
578 done automatically by the simple coding. Imposing the symmetric boundary
579 conditions requires $U_{n,F}=U_{n,B}$ and $U_{\tau,F} = U_{\tau,B}$. We can copy populations
580 in the certain order to do it, for example $f_{B,i} = f_{F,\bar{i}}$, where c_i and $c_{\bar{i}}$ are
581 complementary directions, where $c_{i,n} = -c_{\bar{i},n}$ and $c_{i,\tau} = c_{\bar{i},\tau}$, where $c_{i,n} =$
582 $(\mathbf{c}_i \cdot \mathbf{n})\mathbf{n}$ and $c_{i,\tau} = \mathbf{c}_i - (\mathbf{c}_i \cdot \mathbf{n})\mathbf{n}$.

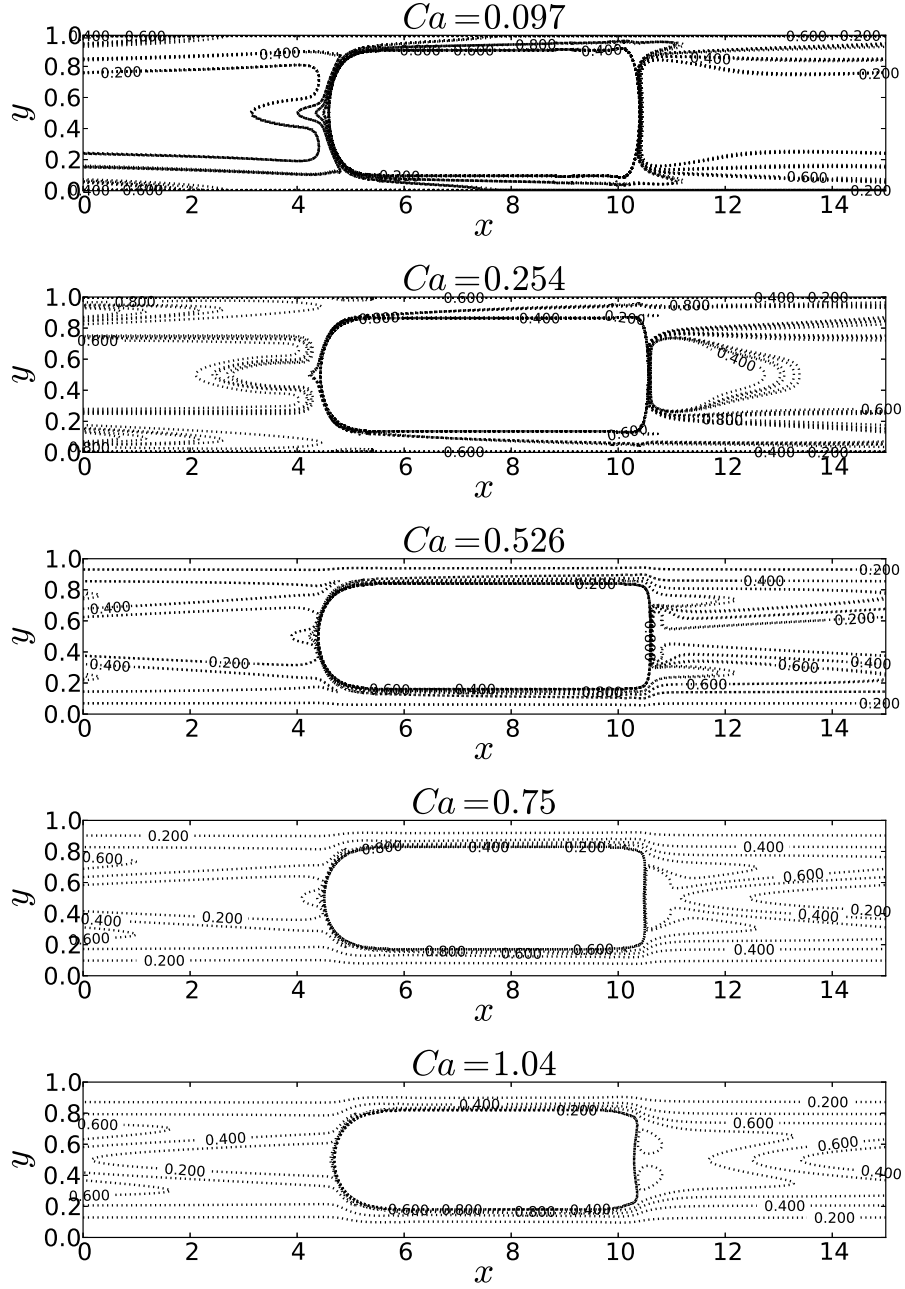


Figure 8: Concentration contour profiles for velocity scalings as identified in Table ?? (top to bottom: $Ca = 0.097, 0.254, 0.526, 0.750, 1.040$). Lines correspond to all different scales indicated in Table ?? (top to bottom: 6 scalings, 5 scalings, 2 scalings, 1 scaling, 1 scaling). Some lines are indistinguishable showing that simulations with velocity scalings are consistent.

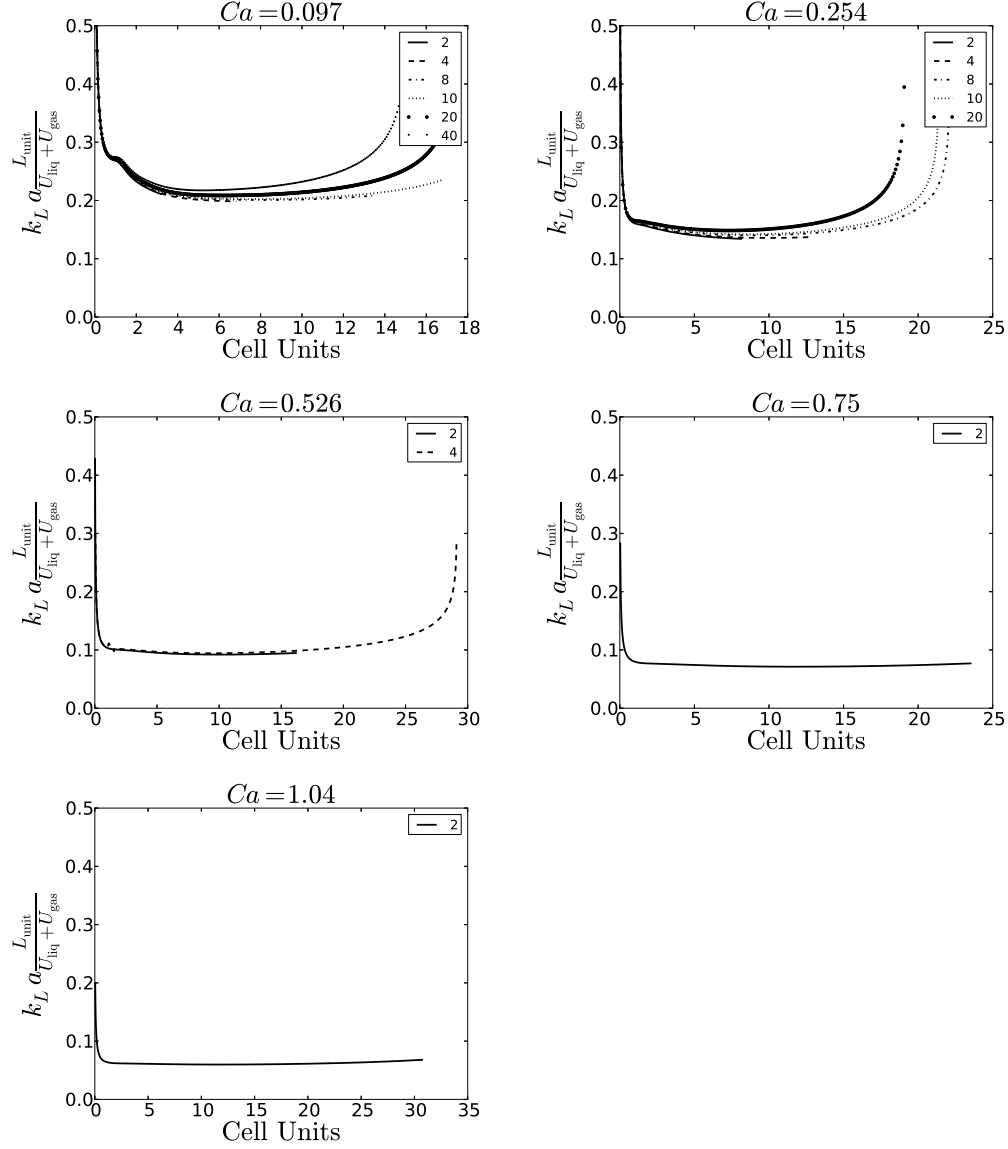


Figure 9: Volumetric mass transfer coefficient for different capillary numbers and scales against the bubble travel distance in the laboratory frame. "Cell Units" axis refers to the physical distance of how many unit cells the bubble travels until the steady state is reached. A legend is provided for velocity scalings. All of them show a good agreement. One can see an abnormal rise of the mass transfer coefficient when the average concentration is close to C^* due to the logarithmic function evaluation. Table ?? summarizes results presented here.

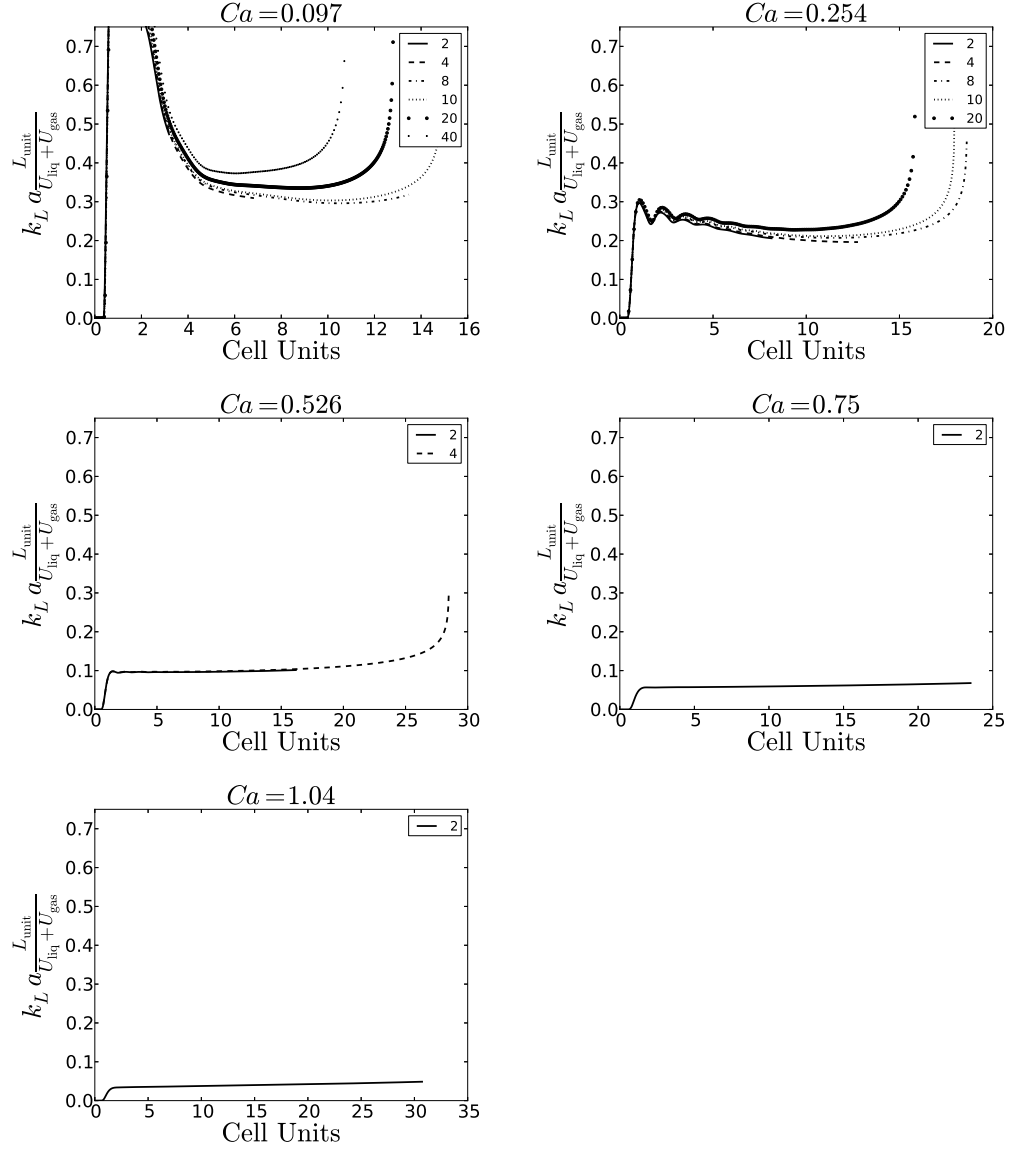


Figure 10: The volumetric mass transfer coefficient with the characteristic concentration based on the inlet/outlet flux averaged concentration as in [?]. One can see that depending on the velocity pattern, the values are either overpredicted or underpredicted in comparison to values specified in Table ??

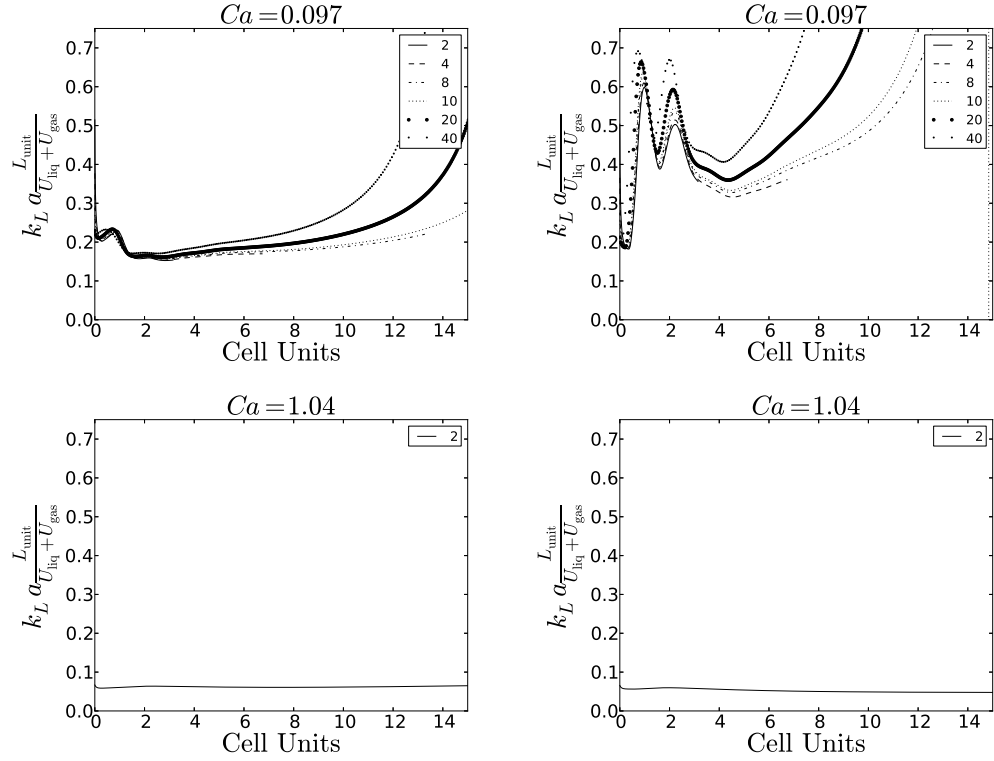


Figure 11: The $\frac{k_L a L_{unit}}{U_{liq} + U_{gas}}$ formulations for $Ca = 0.097$ (top) and $Ca = 1.04$ (bottom) with the characteristic concentration being domain-averaged (left) and inlet/outlet flux-averaged (right). One can see that the $\frac{k_L a L_{unit}}{U_{liq} + U_{gas}}$ formulation produces good results with the characteristic concentration being the average concentration. Moreover, the values are closer to values obtained with many cell simulations, see Fig. ??, than in comparison with periodic boundary simulations in Section ?? . However, the characteristic concentration being inlet/outlet flux-averaged does not produce consistent results.

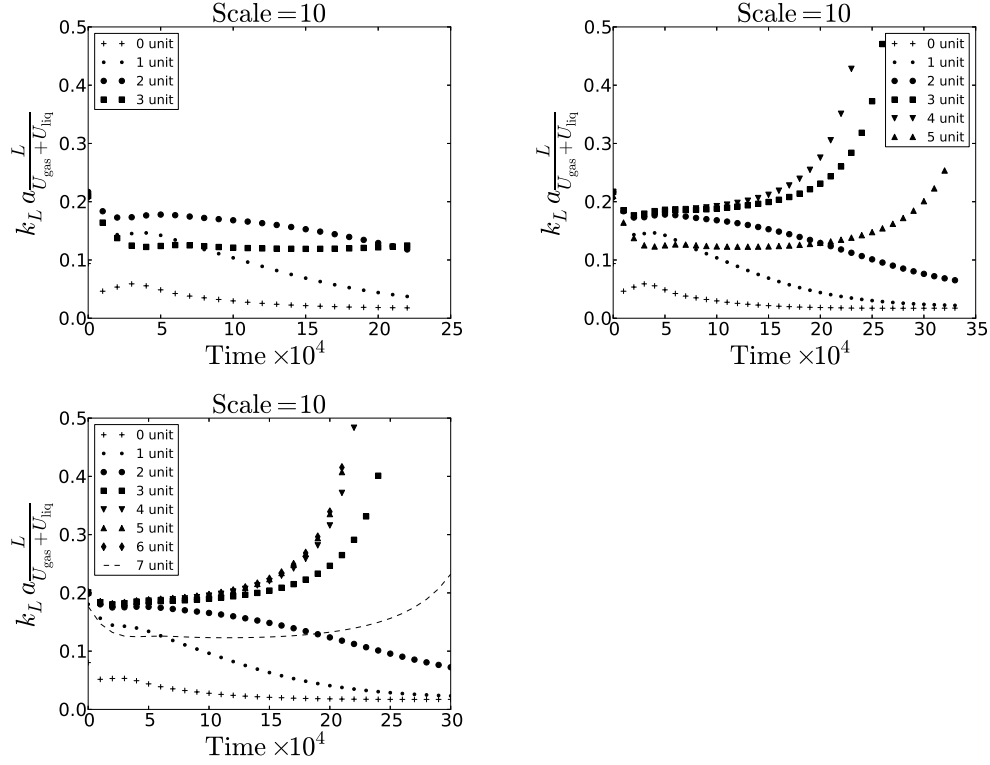


Figure 12: The non-dimensional volumetric mass transfer coefficient defined in Eq. ?? for 4 (top left), 6 (top right), 8 unit cells (bottom). Only scale 10 is presented since all other simulations produce the same results. One can see that 4 unit cells is not enough to avoid the influence of boundaries. However, the results for 6 and 8 unit cells are consistent and show that beginning from third unit cell the results and ending with the penultimate cell results are consistent with periodic boundary simulations and ?] formulations.

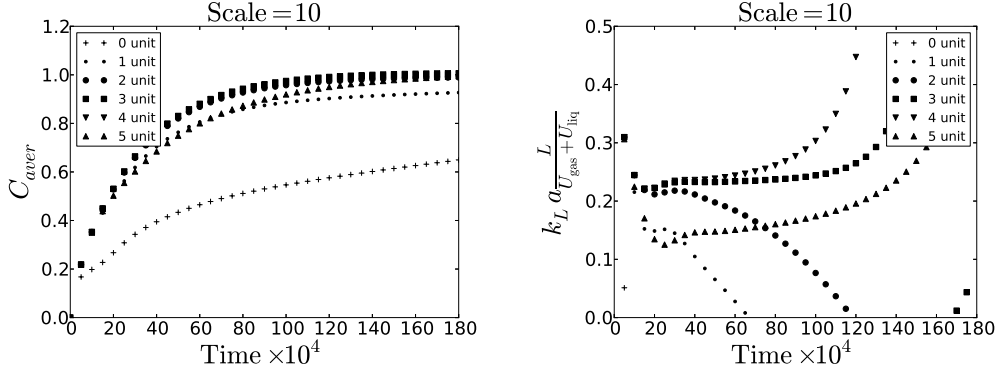


Figure 13: Average concentrations (left) and volumetric coefficients (right) for 6 unit cells. The volumetric mass transfer coefficient is calculated based on Eq. ?? and accounts for inlet and outlet fluxes.

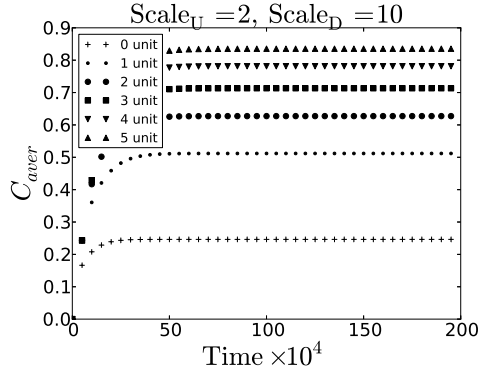


Figure 14: Results for 6 unit cells. The Peclet number equals to $Pe = 2644$. One can see that average concentrations reach certain value and stay constant. Thus, the volumetric mass transfer coefficient, $k_L a \frac{L_{unit}}{U_{bubble} + U_{gas}}$, can be calculated using the spatial approach, see Fig. ??.

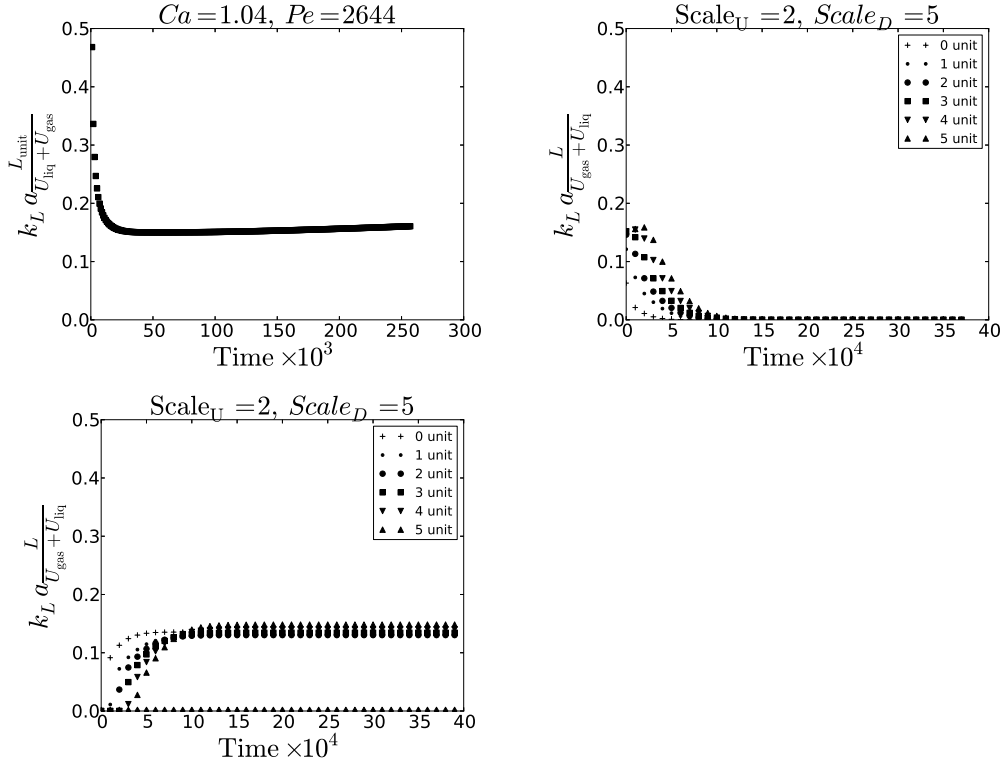


Figure 15: The periodic (top left, 1 unit cell, Eq. ??), unit cells domain-averaged concentrations as a function of time (top right, 6 unit cells, Eq. ??), and spatial location (bottom, 6 unit cells, Eq. ??) calculated volumetric mass transfer coefficients. One can see that they all coincide. However, the calculations based on periodic boundary conditions produce a slightly overestimated volumetric mass transfer coefficient. One can as well see that the domain-averaged concentration simulations (top right) reach the steady volumetric concentration fast and start decaying after that. It is not convenient to use them in practical cases for unmixed slug, i.e. $Ca > 0.7$.

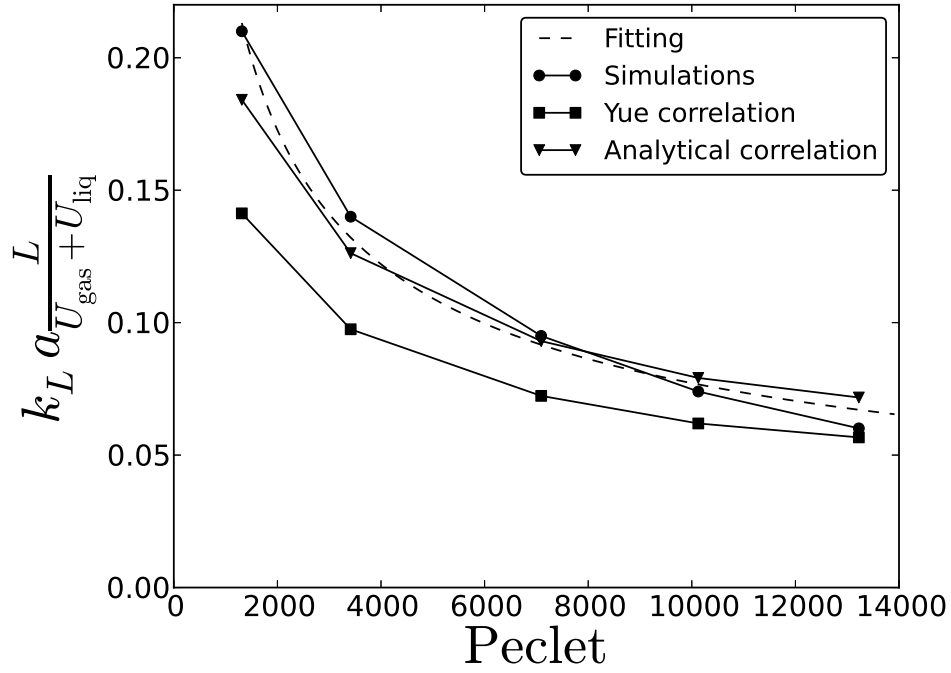


Figure 16: Comparison between the correlation by [?], the analytical correlation derived by following the work [?] and the mass transfer coefficient based on periodic boundary conditions. The fitting curve ($7.745Pe^{-0.50038}$) is proportional to $Pe^{-0.5}$ which corresponds to all correlations. One can as well see that the deviation from the analytical expression becomes larger with the increasing Peclet number, which happens because the analytical expression does not account for the velocity pattern and the bubble shape change.

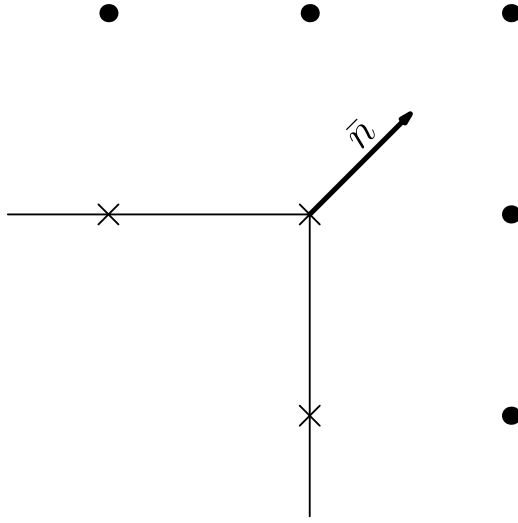


Figure B.17: Free-surface boundary condition represented in the lattice Boltzmann method. Boundary nodes are depicted by crosses, and fluid nodes are represented by dots. The populations at the corner boundary nodes are essentially the populations of the fluid node, but in a different order.